RSC Advances

PAPER

Published on 11 September 2026

Cite this: DOI: 10.1039/d6ra07332h

Design, synthesis, molecular docking and anticancer activity of novel *N*-(4-(chlorodifluoromethoxy)phenyl)-1*H*-pyrrolo[2,3-*b*]pyridine-5-carboxamide derivatives

Pradeep B. Bhise, [ab] Sandeep B. Bhise, [c] Somnath Dasgupta,[b] Ashis Nandy,[b] Rambabu Gundla, [d] Sona Gurska,[ef] Petr Dzubak,[ef] Marian Hajdúch,[ef] Viswanath Das, [ef] Shankar R. Thopate †[g] and Pravin V. Badadhe *[a]

New *N*-(4-(chlorodifluoromethoxy)phenyl)-1*H*-pyrrolo[2,3-*b*]pyridine-5-carboxamide derivatives were designed, synthesised, and evaluated as potential anticancer agents. Among the synthesised derivatives, compound **9c** showed the highest potency against BCR-ABL1-positive K562 leukemia cells, with an IC_{50} of 0.26 ± 0.029 μM, followed by **9a** (0.50 ± 0.005 μM), **9k** (0.64 ± 0.075 μM) and **9l** (0.69 ± 0.11 μM). Importantly, compounds **9a**, **9c** and **9k** showed selectivity for leukemia cells and low toxicity to normal fibroblasts (IC_{50} > 50 μM), with selectivity indices of 100–192. Docking analysis showed that the designed analogues preserved the key pharmacophoric interactions of Asciminib, with compound **9k** showing the best docking score (−42.07 kcal mol^{-1}), followed by **9a** (−40.44 kcal mol^{-1}), compared with Asciminib (−40.13 kcal mol^{-1}). Taken together, these results suggest that the *N*-(4-(chlorodifluoromethoxy)phenyl)-1*H*-pyrrolo[2,3-*b*]pyridine-5-carboxamide scaffold is a useful template for designing selective BCR-ABL1-directed anticancer agents, with compound **9c** as an encouraging lead for further optimisation and mechanistic studies.

Received 7th August 2026
Accepted 2nd September 2026

DOI: 10.1039/d6ra07332h

rsc.li/rsc-advances

Introduction

Chronic myeloid leukaemia (CML) is a clonal myeloproliferative disorder characterised by constitutive activation of the Breakpoint Cluster Region-Abelson murine leukaemia viral oncogene homolog 1 (BCR-ABL1) fusion tyrosine kinase, leading to uncontrolled proliferation of haematopoietic stem cells.[1] It is caused by a reciprocal translocation between chromosomes 9 and 22, known as the Philadelphia chromosome (Ph), which creates the oncogenic BCR-ABL1 fusion gene.[2] The fusion protein BCR-ABL1 has constitutive tyrosine kinase activity, resulting in the activation of several downstream pathways, such as PI3K/AKT, RAS/MAPK and JAK/STAT, which regulate cell proliferation, angiogenesis, apoptosis and resistance to apoptosis.[3] The discovery of BCR-ABL1 as the molecular driver of chronic myeloid leukaemia (CML) revolutionised targeted cancer therapy and established kinase inhibition as a successful therapeutic strategy in oncology. The introduction of selective BCR-ABL1 inhibitors has significantly improved patient survival and transformed CML from a fatal malignancy into a chronic disease. Despite this clinical success, resistance to currently available inhibitors and adverse effects remain major therapeutic challenges, and there is a continuous need to develop novel BCR-ABL1 inhibitors with enhanced potency and selectivity.

Imatinib mesylate, a first-generation tyrosine kinase inhibitor (TKI), was the first targeted therapeutic approved for the treatment of CML and demonstrated efficacy by specifically inhibiting the ATP-binding site of the BCR-ABL1 kinase. Imatinib has become the standard first-line therapy for chronic-phase CML, and significant hematologic and cytogenetic responses have been observed.[4,5] However, prolonged imatinib treatment leads to acquired resistance, which is associated with point mutations within the BCR-ABL1 kinase domain. These

[a]*Department of Chemistry, R B Narayanrao Borawake College, Shrirampur, Ahilyanagar, Maharashtra, 413 709, India. E-mail: pvbadadhe@gmail.com*

[b]*Aragen Life Sciences Ltd, Survey No. 125 and 126, IDA, Mallapur, Hyderabad, Telangana, 500 076, India*

[c]*M.V.P. Samaj, Nashik G.M.D. Arts, B.W. Commerce and Science College, Sinnar, Nashik, Maharashtra, 422 103, India*

[d]*Department of Chemistry, School of Science, GITAM University, Hyderabad 502102, Telangana, India*

[e]*Institute of Molecular and Translational Medicine, Faculty of Medicine and Dentistry, Palacký University and University Hospital Olomouc, Hnevotínska 1333/5, Olomouc, 779 00, Czech Republic*

[f]*Institute of Molecular and Translational Medicine, Czech Advanced Technologies and Research Institute, Palacký University Olomouc, Krízkovskeho 511/8, Olomouc, 779 00, Czech Republic*

[g]*Department of Chemistry, Radhabai Kale Mahila Mahavidyalaya, Tarakpur, Ahilyanagar, Maharashtra, 414001, India*

† Co-guide/Co-supervisor.

limitations prompted the development of second- and third-generation TKIs, including dasatinib, nilotinib, bosutinib, and ponatinib, which exhibit improved activity against several imatinib-resistant BCR-ABL1 mutations.[6]

Second-generation inhibitors showed better efficacy, but resistance and toxicity remain clinically significant. Ponatinib is a third-generation TKI active against the T315I mutation and has shown potent antileukemic activity, but its clinical use is associated with cardiovascular complications and vascular toxicity.[7] Other BCR-ABL1 inhibitors can also cause myelosuppression, hepatotoxicity, pleural effusions, and off-target kinase inhibition. Therefore, developing structurally novel inhibitors with minimal side effects remains an important goal in medicinal chemistry and targeted drug discovery. Previous work has focused on designing hybrid heterocyclic scaffolds and structurally optimised kinase inhibitors to enhance binding affinity, selectivity, and pharmacological properties.

Nitrogen-containing fused heterocyclic systems are well known as privileged scaffolds in medicinal chemistry because they can form favourable hydrogen bonding, π–π stacking, and hydrophobic interactions within kinase active sites. The pyrrolo [2,3-*b*]pyridine nucleus is structurally similar to purine-based systems and can efficiently occupy the ATP-binding pocket of protein kinases.[8] Several pyrrolo-pyridine-containing compounds have been reported as potent inhibitors of receptor and non-receptor tyrosine kinases involved in cancer progression. Modifications at different positions of this scaffold, especially at the carboxamide and aryl substitution sites, can significantly affect kinase selectivity and anti-cancer activity.[9]

Carboxamide-containing heterocycles are another important class of kinase inhibitors because they can form hydrogen-bonding interactions in the ATP-binding region of kinases. The carboxamide functionality can often both donate and accept hydrogen bonds, thereby improving selectivity and binding stability. Aryl carboxamide derivatives have been shown to potently inhibit several oncogenic kinases, including EGFR, BTK, VEGFR and BCR-ABL1.[10] In general, fluorinated carboxamide derivatives exhibit better bioavailability and metabolic stability than their non-fluorinated analogues. The results support the design of novel *N*-(4-(chlorodifluoromethoxy) phenyl)-1*H*-pyrrolo[2,3-*b*]pyridine-5-carboxamide derivatives as potential anticancer agents targeting the BCR-ABL1 kinase.

In this context, the present study was designed to synthesise and evaluate new derivatives of *N*-(4-(chlorodifluoromethoxy) phenyl)-1*H*-pyrrolo[2,3-*b*]pyridine-5-carboxamide as potent inhibitors of BCR-ABL1 kinase. The compounds were characterised for their structures and subjected to molecular docking to explore the interaction pattern within the active site of BCR-ABL1 kinase. The derivatives were also evaluated for cytotoxic efficacy against selected cancer cell lines to assess their anticancer potential. In the present study, we aim to establish a correlation among structural modifications, docking interactions and biological activity, which will shed light on the development of novel pyrrolo-pyridine-based anticancer agents with enhanced therapeutic potential against BCR-ABL1-driven malignancies.

Results and discussion

Rational design

Asciminib was primarily guided by the first-in-class allosteric BCR-ABL1 inhibitor strategy reported by Schoepfer *et al.*[11] It binds to the myristoyl pocket of ABL1, the hydrophobic C-lobe cavity normally occupied by the N-terminal myristoyl group of native ABL1, thereby locking the kinase in an inactive conformation and suppressing downstream oncogenic signalling. Structural studies show that this binding induces a conformational shift in the kinase domain's C-terminal α-helix, promoting docking of the SH3 and SH2 regulatory domains and stabilising the autoinhibited state of BCR-ABL1.[12,13]

Chemically, Asciminib features a pyridine-3-carboxamide core with a 4-(chlorodifluoromethoxy)phenyl group attached to the amide nitrogen. The pyridine ring bears a (3*R*)-3-hydroxypyrrolidin-1-yl substituent and a 1*H*-pyrazol-3-yl group, both positioned adjacent to each other. The chlorodifluoromethoxyphenyl moiety occupies the hydrophobic core of the myristoyl pocket and is the primary determinant of binding affinity; the hydroxypyrrolidine confers favourable physicochemical and pharmacokinetic properties without directly engaging the pocket; and the pyrazolylpyridine carboxamide scaffold positions these groups within the binding cleft. Replacing the chlorodifluoromethoxy group with trifluoromethoxy, or the pyrazolyl substituent with pyrimidine, as reflected in the IC_{50} shifts reported for lead compound **7** and compound **16**.[14] Complementary structural insights come from Mulik *et al.* (2024a), who characterised the biologically active compounds **4c**, **4e**, and **4m**, and from Bhise *et al.* (2026b).[15] These studies highlight the effectiveness of pyrazolo-fused heterocyclic scaffolds for kinase targeting, owing to their planarity, favourable electronic distribution, and capacity for π–π stacking and hydrogen bonding. Incorporating substituted phenyl carboxamide moieties further enhances potency, underscoring their role in stabilising ligand–protein interactions within the kinase-binding pocket.

A new series of 3-substituted-*N*-(4-(chlorodifluoromethoxy) phenyl)-1*H*-pyrrolo[2,3-*b*]pyridine-5-carboxamide derivatives (**8a–p**) was designed as potential allosteric inhibitors of BCR-ABL1. The pyrrolo[2,3-*b*]pyridine core was retained from our earlier lead **9c** and serves as a bicyclic bioisostere of Asciminib's separate pyridine/hydroxypyrrolidine/pyrazole pharmacophore, condensing three interacting elements into a single fused, planar scaffold. This design is proposed to preserve favourable positioning within the myristoyl pocket, though the specific hydrogen-bonding contacts remain to be established through docking studies. The carboxamide linkage, carried over unchanged from both Asciminib and **9c**, provides the conformational constraint known to be necessary for productive pocket engagement. The 4-(chlorodifluoromethoxy)phenyl group remains the primary anchor within the hydrophobic subpocket, consistent with its role in both parent compounds. The chlorodifluoromethoxy substituent is expected to enhance metabolic stability, though this has not yet been measured in the present series. At the C3 position, the pyrazole in **9a** and **9c**

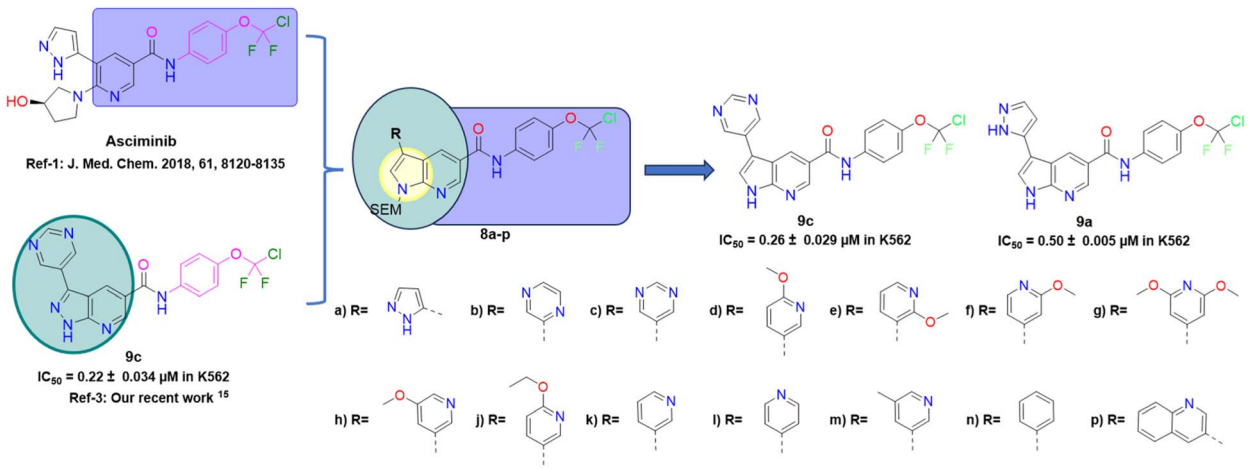

Fig. 1 Rational design and structural optimisation of novel *N*-(4-(chlorodifluoromethoxy)phenyl)-1*H*-pyrrolo[2,3-*b*]pyridine-5-carboxamide derivatives based on the Asciminib scaffold, yielding potent anticancer candidates.

was systematically replaced across **8a–p** to probe whether the pyrazole's contribution to binding, apparently sensitive to regiochemistry given the ~2-fold potency loss from **9c** to its regiochemical analogue **9a**, can be matched or improved by alternative heterocycles varying in nitrogen count and position (pyrimidine, mono- and dimethoxypyridines), added polarity (ethoxy/methoxy-pyridines), or increased ring size and lipophilicity (phenyl, quinoline). This positions the series as a focused SAR study of C3 substituent tolerance, built on the validated **9c** scaffold, rather than as a *de novo* hybridisation of two independent pharmacophores (Fig. 1).

Chemistry

To introduce a methyl ester functionality, the linear synthesis began with palladium-catalysed carbonylation of 5-bromo-1*H*-pyrrolo[2,3-*b*]pyridine (**1**). Methyl 1*H*-pyrrolo[2,3-*b*]pyridine-5-carboxylate (**2**) was obtained quantitatively by reacting compound **1** with Et_3N in methanol at 100 °C under carbon monoxide (300 psi) in the presence of the Pd(dppf)Cl_2·DCM complex. The ^{1}H NMR spectrum showed the ester methoxy signal at 3.89 ppm, and the ^{13}C NMR spectrum showed the carbonyl carbon at 166.39 ppm. Compound **3** was obtained in 63.08% yield by iodinating compound **2** with *N*-iodosuccinimide (NIS) in acetone at room temperature for 1 hour.

The pyrrole nitrogen of compound **3** was protected with an SEM (2-trimethylsilylethoxymethyl) group to improve solubility and to facilitate downstream reactions. The carboxylic acid intermediate was obtained by controlled hydrolysis after protection with SEM-Cl and NaH in DMF (**5**). Characteristic NMR signals, including the carboxylic acid proton at 13.17 ppm and the trimethylsilyl resonance at −0.11 ppm, confirmed successful synthesis (Scheme 1).

Using HATU and Et_3N in DMF, molecule **5** was coupled with 4-(chlorodifluoromethoxy)aniline (**6**) to afford the key intermediate **7** in 83.20% yield. Analogues **8a–p** were prepared *via* Suzuki–Miyaura cross-coupling of compound **7** with various heteroaryl and aryl boronic acids/esters, using the Pd(dppf)Cl_2·DCM complex and K_3PO_4 in dioxane–water. The target compounds **9a–p** were obtained after final deprotection of the SEM group using trifluoroacetic acid. These compounds were

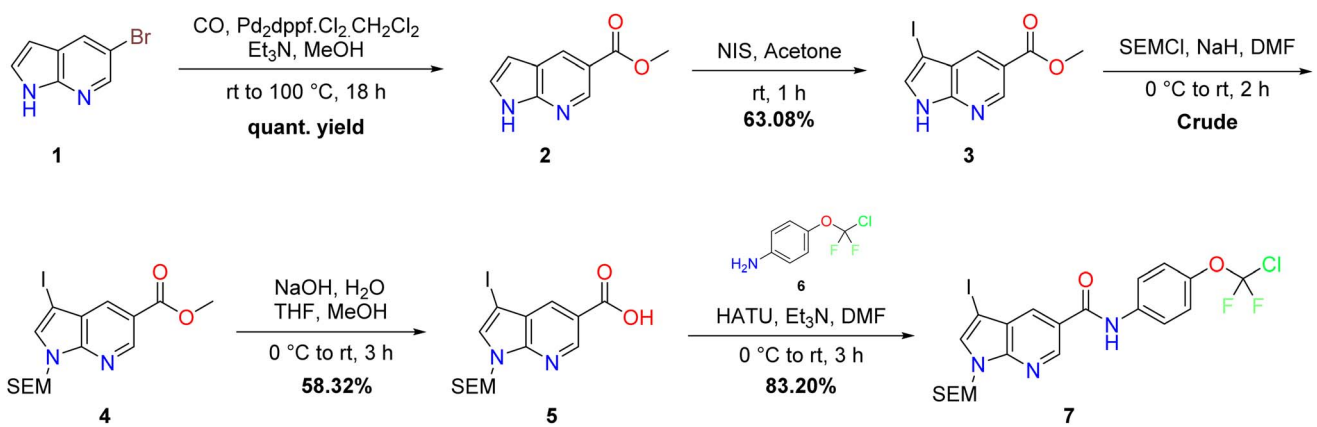

Scheme 1 Synthesis of building block compound **7**.

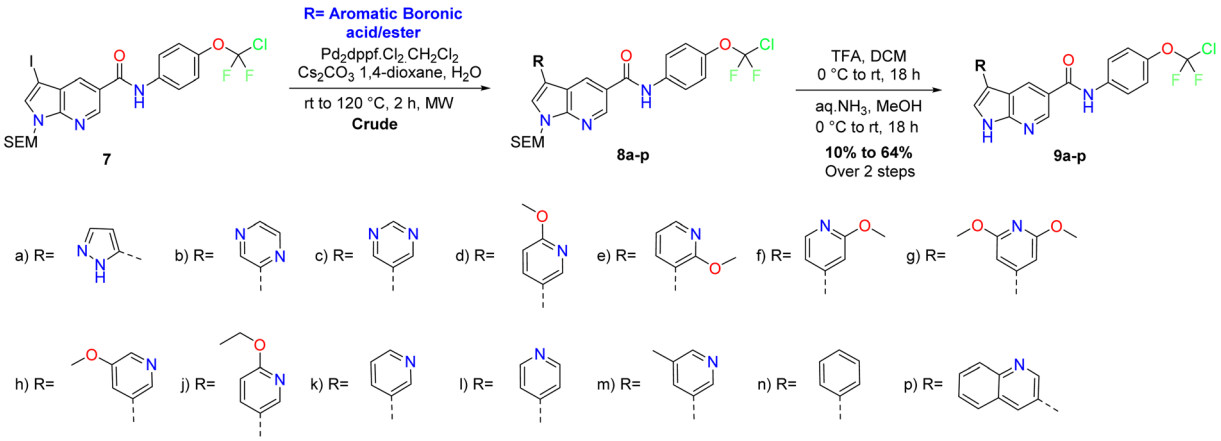

Scheme 2 Synthesis of compound **8a–p** and **9a–p**.

then purified and thoroughly characterised using spectroscopic methods (Schemes 1 and 2).

Biology

The synthesized *N*-(4-(chlorodifluoromethoxy)phenyl)-1*H*-pyrrolo[2,3-*b*]pyridine-5-carboxamide derivatives (**9a–9p**) were evaluated for their cytotoxic activity against a panel of human cancer cell lines, including K562 (BCR-ABL1-positive chronic myeloid leukemia), A549 (lung adenocarcinoma), CCRF-CEM (acute lymphoblastic leukemia), HCT116 and HCT116 $p53^{-/-}$ (colorectal carcinoma), and U2OS (osteosarcoma). Cytotoxicity against normal human fibroblast cell lines (BJ and MRC-5) was also evaluated to assess the compounds' selectivity. Asciminib served as the reference BCR-ABL1 inhibitor. Among the synthesized derivatives, compound **9c** showed the highest cytotoxic activity against the K562 leukemia cell line, with an IC_{50} of 0.26 ± 0.029 μM, followed by **9a** (0.50 ± 0.005 μM), **9k** (0.64 ± 0.075 μM) and **9l** (0.69 ± 0.11 μM). Although these compounds were less potent than the reference drug Asciminib (0.005 ± 0.001 μM), they exhibited activity in the submicromolar range, indicating that the 1*H*-pyrrolo[2,3-*b*]pyridine scaffold is highly favourable for BCR-ABL1 inhibition.

Compounds **9a** and **9c** showed selectivity for K562 cells and exhibited very low toxicity toward normal fibroblasts (BJ and MRC-5; IC_{50} > 50 μM). Consequently, compound **9c** showed a selectivity index (SI = 192.31 for both BJ and MRC-5), whereas **9a** also demonstrated exceptional selectivity with an SI of 100. Similarly, compound **9k** showed selectivity (SI = 78.13) and potent inhibition of K562, indicating that these derivatives preferentially target leukemia cells over normal cells. Among the compounds tested, **9l** was the most potent against the CCRF-CEM leukemia cell line, with an IC_{50} of 2.98 ± 0.51 μM, followed by **9a** (7.12 ± 1.30 μM), **9d** (7.84 ± 1.31 μM), **9f** (8.58 ± 1.22 μM) and **9g** (9.17 ± 1.04 μM). The other compounds showed moderate to weak activity, and compound **9c** was practically inactive against CCRF-CEM (IC_{50} > 50 μM), suggesting that structural modifications affect activity differently across leukemia types.

Evaluation in solid tumour cell lines showed that most derivatives exhibited moderate cytotoxicity. Among the compounds, **9j** was the most active, with an IC_{50} of 8.24 ± 1.15 μM, followed by **9l** (11.12 ± 1.95 μM) in the A549 lung cancer model. Other analogues displayed IC_{50} values of 18–31 μM or were inactive (>50 μM). Compounds **9b** and **9k** showed negligible activity against A549 cells (IC_{50} > 50 μM), indicating selectivity for hematological malignancies. In the HCT116 colorectal cancer model, compound **9l** also showed the highest potency (IC_{50} = 5.25 ± 0.32 μM), whereas compounds **9d** (16.21 ± 2.38 μM), **9g** (16.77 ± 2.30 μM), and **9p** (21.09 ± 3.27 μM) showed moderate activity. A comparable trend was observed when tested against the HCT116 $p53^{-/-}$ cell line, with **9l** again showing inhibition (IC_{50} = 5.37 ± 0.39 μM), suggesting that its cytotoxicity is largely independent of p53 status. Compounds **9d**, **9g**, **9j** and **9p** also showed moderate activity in p53-deficient cells.

The most cytotoxic compound was **9j**, with an IC_{50} of 7.81 ± 1.93 μM, followed by **9l** (8.28 ± 0.97 μM) and **9p** (10.49 ± 2.26 μM) in the osteosarcoma cell line U2OS. The remaining derivatives showed moderate activity, while compounds **9b** and **9k** were comparatively less active. Almost all derivatives showed low toxicity in cytotoxicity evaluations using normal fibroblast cell lines. Compounds **9a**, **9b**, **9c**, **9d** and **9k** showed IC_{50} values >50 μM in both BJ and MRC-5 cells, thereby confirming their safety profile. Conversely, compound **9j** showed relatively higher toxicity towards normal cells (BJ = 11.01 ± 1.83 μM; MRC-5 = 17.90 ± 4.54 μM), with SI values of only 1.07 and 1.74, respectively, indicating poor selectivity despite its activity against certain solid tumors. Additionally, compound **9p** showed low selectivity (SI = 0.59–1.24), indicating limited therapeutic potential.

Evaluation in solid tumor cell lines showed that most derivatives exhibited moderate cytotoxicity. Among the compounds, **9j** was the most active, with an IC_{50} of 8.24 ± 1.15 μM, followed by **9l** (11.12 ± 1.95 μM) in the A549 lung cancer model. Other analogues displayed IC_{50} values of 18–31 μM or were inactive (>50 μM). Compounds **9b** and **9k** showed negligible activity against A549 cells (IC_{50} > 50 μM), suggesting

Table 1 Cytotoxicity (IC_{50}, μM) of compounds **9a–9p** and Asciminib tested across BCR-ABL1-positive K562 cells, other cancer cell lines, normal human fibroblasts, and selectivity index (SI). Data are presented as mean ± SD from at least six independent biological experiments ($n \geq 6$)

Cancerous cell lines							Non-cancerous cell lines		SI index	
Compound (purity)	K562	A549	CCRF-CEM	HCT116	HCT116 $p53^{-/-}$	U2OS	BJ	MRC-5	SI (BJ)	SI (MRC-5)
9a (95.09%)	0.50 ± 0.01	30.95 ± 3.09	7.12 ± 1.30	32.53 ± 5.92	24.16 ± 2.82	20.23 ± 2.87	>50	>50	100	100
9b (96.01%)	1.10 ± 0.25	>50	27.24 ± 4.05	42.62 ± 4.89	39.70 ± 4.51	44.11 ± 2.44	>50	>50	45.5	45.5
9c (99.75%)	0.26 ± 0.03	27.59 ± 2.69	>50	34.02 ± 2.96	35.42 ± 3.54	24.79 ± 4.63	>50	>50	192	192
9d (93.67%)	2.56 ± 0.57	22.43 ± 6.23	7.84 ± 1.31	16.21 ± 2.38	11.24 ± 1.66	13.56 ± 1.53	>50	>50	19.5	19.5
9e (97.51%)	4.40 ± 0.70	31.33 ± 2.61	17.39 ± 4.58	30.05 ± 1.05	29.46 ± 1.58	27.62 ± 3.63	38.38 ± 10.31	39.45 ± 4.97	8.72	8.97
9f (99.02%)	4.13 ± 0.46	24.21 ± 3.20	8.58 ± 1.22	24.25 ± 2.64	20.72 ± 0.81	24.93 ± 2.70	25.46 ± 2.27	25.55 ± 2.22	6.16	6.19
9g (99.64%)	5.53 ± 0.98	20.61 ± 3.58	9.17 ± 1.04	16.77 ± 2.30	12.36 ± 1.04	14.45 ± 2.26	42.06 ± 7.57	>50	7.61	9.04
9h (99.09%)	1.92 ± 0.44	21.92 ± 4.58	12.88 ± 1.29	31.69 ± 7.24	16.00 ± 3.24	20.77 ± 1.70	21.90 ± 4.40	38.50 ± 6.81	11.4	20.1
9j (98.92%)	10.26 ± 1.18	8.24 ± 1.15	10.29 ± 3.16	26.08 ± 3.01	15.24 ± 1.93	7.81 ± 1.93	11.01 ± 1.83	17.90 ± 4.54	1.07	1.74
9k (99.14%)	0.64 ± 0.08	>50	30.01 ± 8.04	>50	>50	36.37 ± 6.42	>50	>50	78.1	78.1
9l (98.63%)	0.69 ± 0.11	11.12 ± 1.95	2.98 ± 0.51	5.25 ± 0.32	5.37 ± 0.39	8.28 ± 0.97	18.79 ± 3.18	22.38 ± 1.07	27.2	32.4
9m (93.18%)	2.27 ± 0.51	20.43 ± 3.43	12.21 ± 1.21	25.12 ± 1.85	20.99 ± 3.00	17.60 ± 4.04	27.48 ± 2.74	27.72 ± 4.90	12.1	12.2
9n (99.57%)	6.80 ± 1.22	18.92 ± 2.60	10.99 ± 2.07	23.21 ± 1.96	22.47 ± 4.05	20.97 ± 3.26	28.69 ± 1.32	27.51 ± 3.52	4.22	4.05
9p (98.77%)	23.51 ± 2.53	19.09 ± 4.52	18.38 ± 1.65	21.09 ± 3.27	10.73 ± 1.72	10.49 ± 2.26	13.83 ± 1.78	29.12 ± 8.20	0.59	1.24
Asciminib	0.010 ± 0.001	42.99 ± 3.46	16.11 ± 3.31	28.31 ± 2.71	26.74 ± 2.71	33.34 ± 3.43	>50	>50	>10 000	>10 000

selectivity towards hematological malignancies. In the HCT116 colorectal cancer model, compound **9l** also showed the highest potency ($IC_{50} = 5.25 \pm 0.32$ μM), whereas compounds **9d** (16.21 ± 2.38 μM), **9g** (16.77 ± 2.30 μM) and **9p** (21.09 ± 3.27 μM) showed moderate activity. A comparable trend was observed in the HCT116 $p53^{-/-}$ cell line, with **9l** again showing inhibition ($IC_{50} = 5.37 \pm 0.39$ μM).

To summarise, a biological evaluation indicated that compounds **9c**, **9a**, **9k** and **9l** are promising derivatives. Among them, compound **9c** exhibited the best balance of potency and selectivity, showing sub-micromolar activity against BCR-ABL1-positive K562 cells ($IC_{50} = 0.26$ μM) and a high selectivity index of 192. Among the tested compounds, **9c** is one of the best lead compounds for further optimisation, whereas **9l** showed the broadest spectrum of anticancer activity against both hematological and solid tumor cell lines, with acceptable selectivity for normal fibroblasts. The results suggest that *N*-(4-(chlorodifluoromethoxy)phenyl)-1*H*-pyrrolo[2,3-*b*]pyridine-5-carboxamide is a promising template for designing and developing selective anticancer agents against BCR-ABL1-positive leukemia (Table 1).

Molecular docking

The molecular docking protocol was validated by re-docking the co-crystallised inhibitor Asciminib into the allosteric myristoyl-binding pocket of BCR-ABL1 (PDB ID: 5MO4). The docked pose reproduced the experimental crystal conformation with an RMSD of 0.93 Å, confirming the accuracy and robustness of the docking methodology. Asciminib was docked in the characteristic binding orientation within the allosteric pocket, where a conserved structural water molecule mediated three hydrogen-bond interactions with Ala452, Tyr454 and Glu481, thereby stabilising ligand binding. The 4-(chlorodifluoromethoxy)aniline moiety was found to fit into a hydrophobic pocket formed by Leu359, Leu360, Val487 and Ile521, and the pyrazole ring was favourably hydrogen-bonded to the acidic residue Glu481. The pyrrolidin-3-ol group was extended in the direction of the solvent-exposed region with a binding mode close to the crystallographic one.

Docking of the synthesised derivatives (**9a–9p**) reproduced the main pharmacophoric interactions observed for Asciminib.

Table 2 Molecular docking results of the compounds (**9a–9p**) and the reference drug Asciminib docking score (GS, kcal mol^{-1})

Compound name	Docking score (kcal mol^{-1})	Compound name	Docking score (kcal mol^{-1})
9a	−40.44	**9h**	−36.23
9b	−35.96	**9j**	−21.00
9c	−35.83	**9k**	−42.07
9d	−26.13	**9l**	−34.70
9e	−36.63	**9m**	−37.82
9f	−35.40	**9n**	−36.09
9g	−36.18	**9p**	−20.48
Asciminib			−40.13

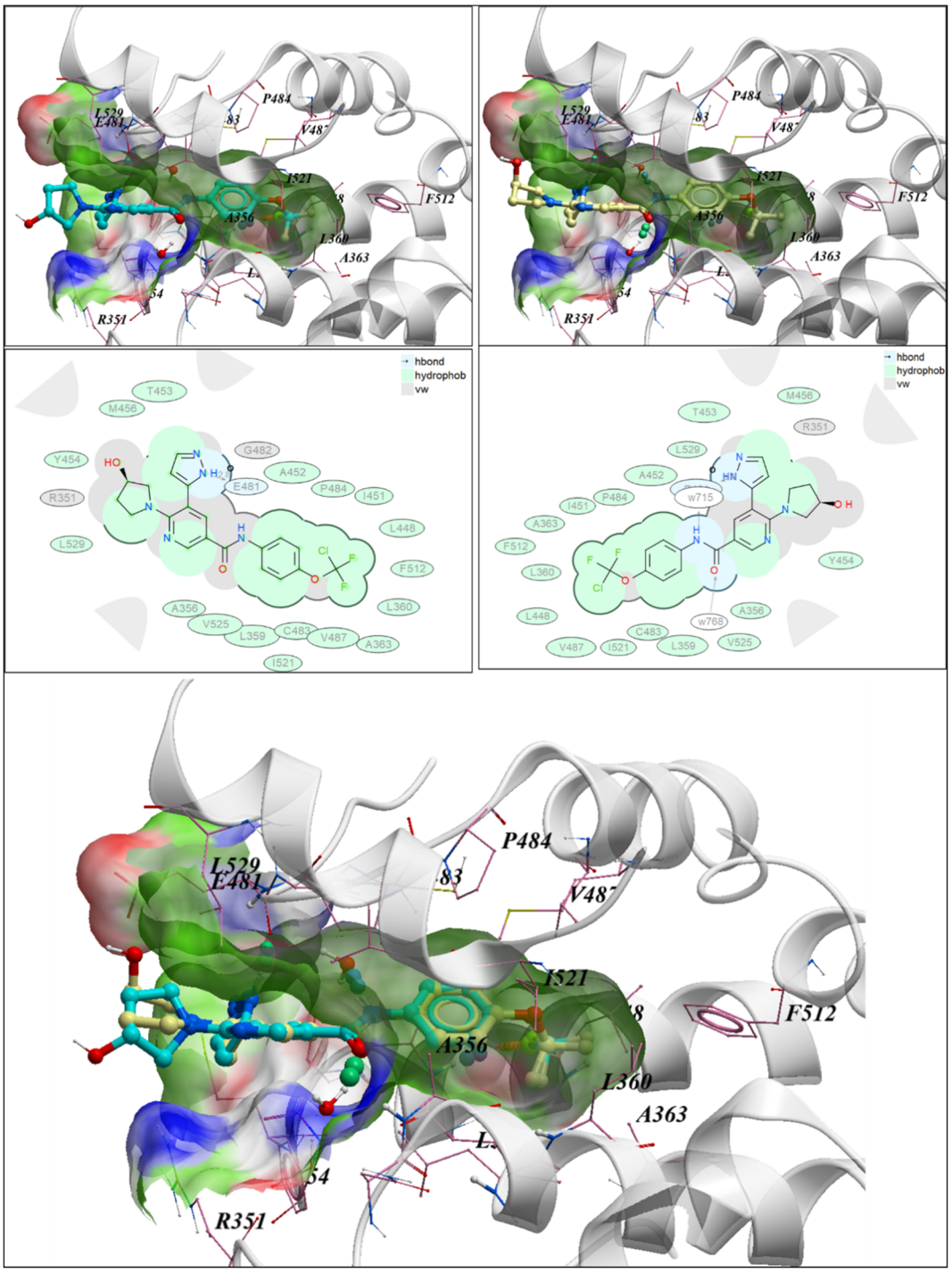

Fig. 2 The binding mode of Asciminib in BCR-ABL1 protein (PDB: 5MO4); overlay of crystal pose w.r.t. the docking pose of Asciminib at the binding site of BCR-ABL1 protein.

Derivative **9k** showed the best docking score (−42.07 kcal mol^{-1}) among the evaluated compounds, surpassing Asciminib (−40.13 kcal mol^{-1}) and **9a** (−40.44 kcal mol^{-1}). Compounds **9m** (−37.82 kcal mol^{-1}), **9e** (−36.63 kcal mol^{-1}), **9h** (−36.23 kcal mol^{-1}), **9g** (−36.18 kcal mol^{-1}), **9n** (−36.09 kcal mol^{-1}), **9b** (−35.96 kcal mol^{-1}), **9c** (−35.83 kcal mol^{-1}), and **9f** (−35.40 kcal mol^{-1}) also showed binding affinity to the allosteric pocket. Structure based analysis revealed that heterocyclic scaffolds with polar nature such as pyrazole (**9a**), pyrazine (**9b**), pyrimidine (**9c**) and pyridine analogues (**9k**) maintained favourable interactions by positioning their heteroatoms in the polar region around Glu481. In contrast, the introduction of less polar substituents such as methyl, methoxy, dimethoxy or

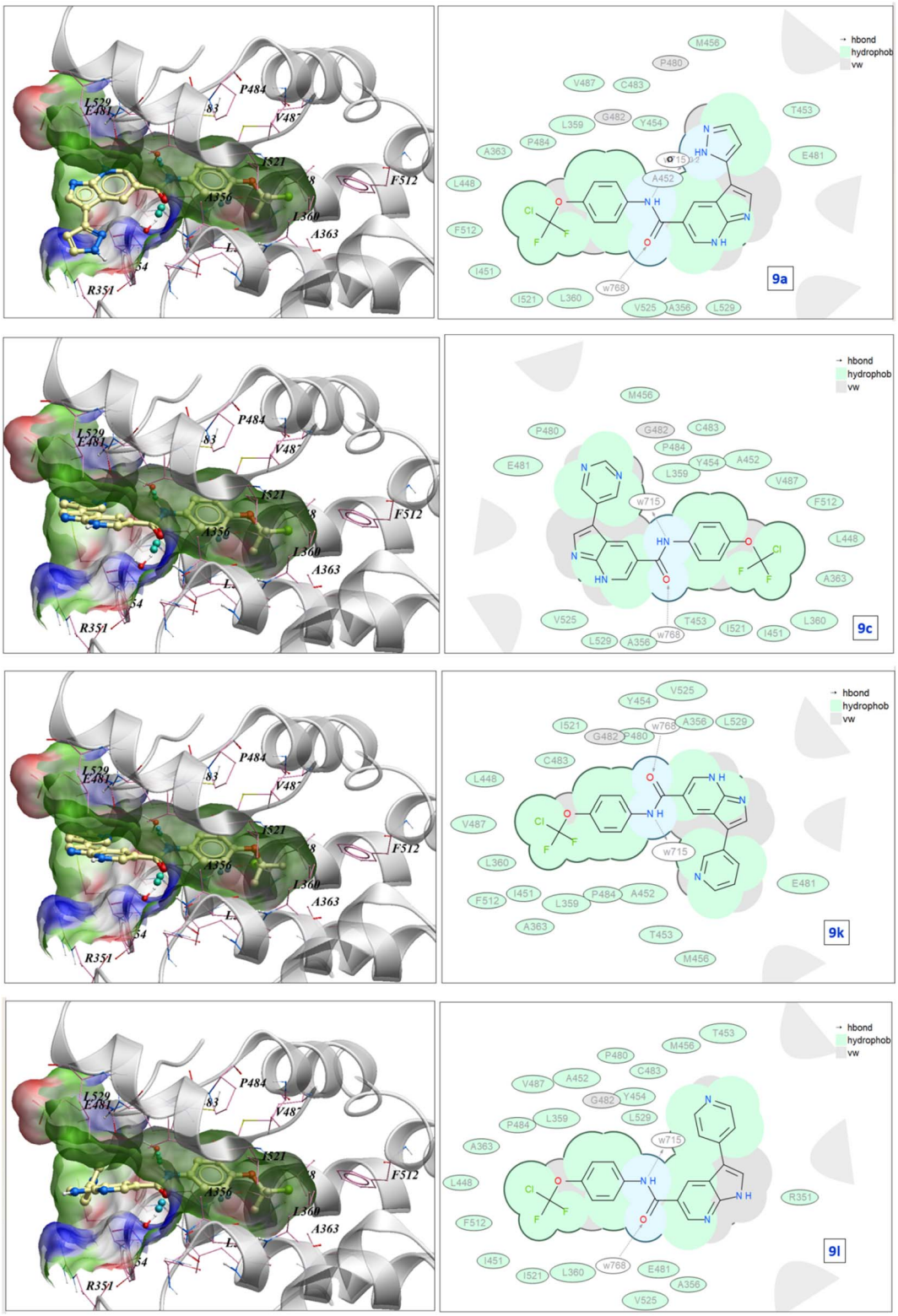

Fig. 3 Molecular docking binding poses of the active *N*-(4-(chlorodifluoromethoxy)phenyl)-1*H*-pyrrolo[2,3-*b*]pyridine-5-carboxamide derivatives in the allosteric myristoyl binding pocket of BCR-ABL1 (PDB ID: 5MO4). The binding conformations of **9a**, **9c**, **9k**, and **9l** are shown within the protein binding cavity. The protein is displayed as a cyan cartoon with the binding pocket represented as a molecular surface, while the ligands are shown as stick models.

ethoxy groups disturbed the best fit and the electrostatic complementarity in the acidic pocket and resulted in a decrease in binding affinity. This effect was more prominent for compounds **9d** (-26.13 kcal mol^{-1}), **9j** (-21.00 kcal mol^{-1}) and **9p** (-20.48 kcal mol^{-1}) with the least docking scores (Table 2). All figures are retained in SI file Fig. 2 and 3. Collectively, these results emphasize the significance of maintaining correct polarity and hydrogen bonding ability around the Glu481 region to achieve optimal recognition in the BCR-ABL1 allosteric binding site.

Molecular dynamics simulations revealed marked differences in the binding behaviour of the active compound **9c** and the inactive compound **9p** (Table S1). The protein backbone RMSD profiles indicated that both complexes remained stable during the initial stages of the 100 ns simulation, with comparable conformational behaviour up to approximately 40 ns (Fig. 4A). Beyond this point, however, the trajectories began to diverge. The **9c**-bound complex underwent a gradual conformational transition, reflected in an increase in RMSD, suggesting an adaptive rearrangement of the protein structure to accommodate the ligand within the binding pocket. Importantly, after approximately 90 ns, the RMSD plateaued, indicating convergence towards a stable and energetically favourable conformational state. In contrast, the **9p**-bound complex continued to show increasing RMSD values throughout the simulation, indicating persistent structural rearrangements without attaining a similarly stabilised conformation. These observations suggest that binding of **9c** promotes the formation of a productive protein conformation, whereas **9p** is less effective at stabilizing the target structure.

To further investigate ligand stability within the binding site, ligand RMSD was monitored throughout the simulation (Fig. 4B). Consistent with the protein RMSD results, **9c** maintained RMSD values predominantly between 0.3 and 1.0 nm, indicating stable retention within the binding pocket while allowing sufficient flexibility for conformational adaptation (Fig. 5A). Conversely, **9p** showed more frequent fluctuations and occasional larger deviations, suggesting a comparatively less stable binding mode (Fig. 5B). The simultaneous stabilization of both protein and ligand RMSD in the **9c** complex indicates coordinated adaptation of the receptor and ligand towards an optimised bound state, whereas the continued fluctuations observed in **9p** reflect weaker stabilisation of the complex.

The enhanced stability of the **9c** complex was further corroborated by receptor–ligand contact analyses (Fig. 4C). Throughout the simulation, **9c** exhibited more favourable interaction energies and maintained a significantly higher number of protein–ligand contacts (approximately 14–21) than **9p** (approximately 12–14). The persistent interaction network formed by **9c** likely stabilises the active protein conformation and reinforces ligand retention within the binding pocket. In contrast, the lower contact occupancy and comparatively weaker interaction energies observed for **9p** suggest reduced interaction with key binding-site residues. Collectively, these findings demonstrate that the superior activity of **9c** arises from its ability to induce a favourable conformational rearrangement of the protein, maintain a stable binding mode, and establish a stronger interaction network, whereas the inactive compound **9p** fails to achieve comparable stabilisation during the simulation.

Discussion

Molecular docking studies were conducted to investigate plausible binding orientations and key ligand–receptor interactions of compounds **9a–9p** within the target protein's active site. The docking results revealed common interaction patterns that may contribute to target recognition and provided a structural basis for interpreting the observed structure–activity relationships. Although docking scores provide an estimate of the relative favourability of the predicted binding poses, they do not necessarily correlate with cellular potency because biological activity is influenced by multiple factors beyond target binding. Therefore, the docking study was used primarily as a qualitative tool to rationalise ligand–protein interactions and support SAR analysis, rather than as a quantitative predictor of antiproliferative activity.

The synthesised *N*-(4-(chlorodifluoromethoxy)phenyl)-1*H*-pyrrolo[2,3-*b*]pyridine-5-carboxamide derivatives showed potent cytotoxicity, particularly against the BCR-ABL1-positive K562 leukaemia cell line, indicating the therapeutic potential of the pyrrolo[2,3-*b*]pyridine scaffold. Among the synthesized compounds, **9c** was the most active ($IC_{50} = 0.26 \pm 0.029$ μM), followed by **9a** (0.50 ± 0.005 μM), **9k** (0.64 ± 0.075 μM), and **9l** (0.69 ± 0.11 μM). Although less active than the reference drug Asciminib ($IC_{50} = 0.005 \pm 0.001$ μM), these compounds showed submicromolar activity and selectivity. In particular, compound **9c** displayed the highest selectivity index (SI = 192.31), followed by **9a** (SI = 100) and **9k** (SI = 78.13), showing a broad therapeutic window and much lower toxicity against normal BJ and MRC-5 fibroblasts (Fig. 2).

Further support for the anticancer potential of this scaffold comes from the work of Narva *et al.*,[16] synthesized a series of pyrrolo[2,3-*b*]pyridine analogs and evaluated them against A549, HeLa and MDA-MB-231 cancer cell lines. Several derivatives exhibited inhibitory activity in the range of 0.12–9.84 μM. These results suggest that appropriately substituted pyrrolo[2,3-*b*]pyridine analogues can provide low-micromolar to submicromolar cellular activity.[17,18]

Off-target toxicity in normal fibroblasts has led many previously reported ATP-competitive kinase inhibitors to have selectivity indices below 20. In contrast, **9c** (SI = 192), **9a** (SI = 100) and **9k** (SI = 78.1) showed much higher selectivity, implying that the chlorodifluoromethoxy substituent may contribute to enhanced discrimination between malignant and normal cells. The improved selectivity could be attributed to enhanced hydrophobic interactions, optimal steric complementarity within the BCR-ABL1 ATP-binding pocket, and beneficial halogen-bonding interactions from the difluoromethoxy group.

However, although the synthesized compounds were less potent than the clinically optimised allosteric inhibitor Asciminib (5 nM), compounds **9c**, **9a**, **9k**, and **9l** are promising early-stage leads for further structural optimisation, given their

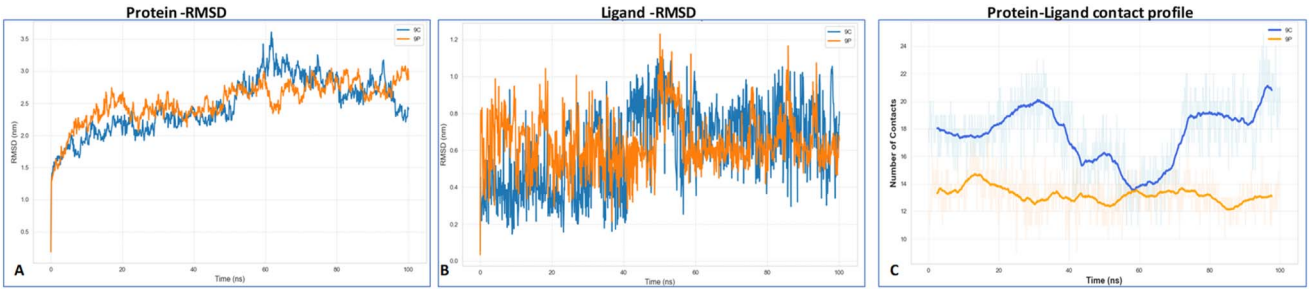

Fig. 4 Protein-RMSD (A), ligand-RMSD (B) and protein-ligand contact profile (C) of active (**9c**) and inactive (**9p**) compounds during 100 ns MD simulation.

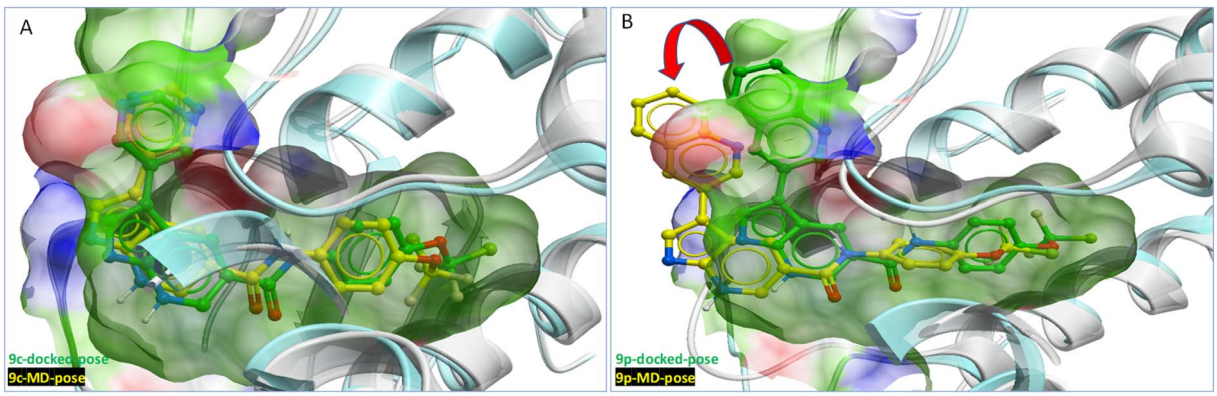

Fig. 5 Alignment of the docked pose and the MD pose (100 ns) of (A) active (**9c**) and (B) inactive (**9p**).

submicromolar cytotoxicity and good selectivity profiles. Further studies, including BCR-ABL1 enzyme inhibition assays, kinase selectivity profiling, molecular docking, molecular dynamics simulations, apoptosis studies, pharmacokinetic evaluation, and *in vivo* efficacy studies, are warranted to establish their potential as next-generation anticancer agents.

Conclusion

In conclusion, the synthesized *N*-(4-(chlorodifluoromethoxy) phenyl)-1*H*-pyrrolo[2,3-*b*]pyridine-5-carboxamide derivatives showed good anticancer activity across the tested cancer cell lines, with particularly strong activity against K562 leukemia cells. Among the derivatives tested, **9c** was the most active against K562 cells, with an IC_{50} of 0.26 ± 0.03 μM and a high selectivity index (SI = 192), followed by **9a** (IC_{50} = 0.50 ± 0.01 μM; SI = 100) and **9k** (IC_{50} = 0.64 ± 0.08 μM; SI = 78.1). Although these compounds were less potent than Asciminib (K562 IC_{50} = 0.010 ± 0.001 μM), their favourable submicromolar activity and preliminary selectivity support their potential as lead structures for further optimisation. Molecular docking and further MD studies provided insights into their possible interactions with the target. Overall, **9c**, **9a**, and **9k** are lead compounds for further structural optimisation, while target-specific, mechanistic, and *in vivo* studies are required to establish their molecular mode of action and therapeutic potential.

Experimental procedure

Chemistry

All chemicals, reagents, catalysts and solvents were procured from BLD pharma (Hyderabad, India), Thermo Fisher Scientific (Hyderabad, India) and Avra Synthesis (Hyderabad, India). All the chemicals, reagents, catalysts and solvents were used as received without further purification or crystallisation. All mentioned yields are isolated yields after purification techniques or crystallization methods. ^{1}H NMR and ^{13}CNMR spectra were logged on a Bruker TOPSPIN-3.5pl7, AVANCE-III HD spectrometers at 400 MHz for ^{1}H-NMR, 376 MHz for ^{13}C-NMR and 100 MHz for ^{19}F-NMR respectively. Chemical shift (δ) is expressed in ppm relative to tetramethylsilane (TMS) as an internal reference compound and $CDCl_3$, DMSO-d_6 were used as a solvent to record the data. Thin layer chromatography was run using commercial silica gel 60 F254 (Merck, Darmstadt, Germany) and visualised under UV light (λ_{max} = 254 or 365 nm). Available ^{1}H NMR spectra were reported in the following format (δ, chemical shift; multiplicity; coupling constants (J) in Hz; number of integrated protons). Splitting of the proton pattern was described using the following abbreviations: broad singlet (brs), singlet (s), doublet (d), triplet (t), quartet (q), doublet of doublets (dd), triplet of doublets (td), quartet of doublets (qd), doublet of triplets (dt), and multiplet (m). HRMS data were obtained using the Model 6540ba Qtof – Infinity 1290 of M/S Agilent Technologies India Pvt. Ltd (NIPER, India). High-

performance liquid chromatography (HPLC) analyses were performed on a Waters Alliance 2996 instrument system equipped with a 2998 PDA MaxPlot (190.0 nm to 800.0 nm) and a 2998 (210–400 nm), and a XBridge Shield C18 column (4.6 × 250 mm, 5 μm). The mobile phase comprised of buffer A (10 mM Ammonium Bicarbonate in Milli-Q water) and buffer B (chromatographic grade CH_3CN). The gradient time *vs.* percentage of CH_3CN ratio was (*T*/% *B*): 0/10, 12/98, 16/98, 16.1/10, 20/10 was applied at a flow rate of 1.0 mL min^{-1} at Ambient temperature. A Waters – Alliance 2996 instrument system equipped with a 2998 PDA MaxPlot (190.0 nm to 800.0 nm) 2998 (210–400 nm) and a Acquity; UPLC; BEH; C18 column (100 mm × 2.1, 1.7 μm). The mobile phase comprised of buffer A (Milli-Q H_2O containing 0.1% trifluoroacetic acid) and buffer B (chromatographic grade CH_3CN). The gradient time *vs.* percentage of CH_3CN ratio was (*T*/% *B*): 0/10, 12/98, 16/98, 16.1/10, 20/10 was applied at a flow rate of 1.0 mL min^{-1} at Ambient temperature. HPLC data is mentioned as percentage purity and retention time (RT) in minutes. Liquid Chromatography-Mass Spectrometry (LC-MS) was obtained from a Waters Acquity-UPLC-SQ Detector-2 mass spectrometer and a AQUITY UPLC BEH C18 1.7 μm, 2.1 × 50 mm at flow rate 0.6 mL min^{-1} at 35 °C with electrospray ionization in either positive (+ESI) or negative (−ESI) mode. Data is expressed as observed mass (*m*/*z*), assignment (M = molecular ion), and relative intensity (%). The mobile phase comprised of buffer A (0.05% formic acid in Milli-Q water) and buffer B (0.05% formic acid in chromatographic grade CH_3CN). The gradient time *vs.* percentage of CH_3CN ratio was (*T*/% *B*): 0/3, 0.3/3, 2.5/98, 3.5/98, 4.0/3, 4.01/3 (ESI). The gradient time *vs.* percentage of CH_3CN ratio was (*T*/% *B*): 0/3, 0.05/3, 1.2/98, 1.6/98, 1.65/3, 2/3 was applied at a flow rate of 1.0 mL min^{-1} at 55 °C temperature. LC-MS data is mentioned as percentage purity and retention time (RT) in minutes.

Methyl 1*H*-pyrrolo[2,3-*b*]pyridine-5-carboxylate (2). To a 10 minute argon-purged, stirred solution of 5-bromo-1*H*-pyrrolo [2,3-*b*]pyridine **1** (10.0 g, 50.75 mmol) in MeOH (200 mL), $Pd(dppf)Cl_2 \cdot DCM$ (4.14 g, 5.07 mmol) and Et_3N (14.12 mL, 101.50 mmol) were added at ambient temperature. The resulting mixture was filled with CO gas (300 psi), heated to 100 °C, and maintained for 18 h. The reaction progress was monitored by TLC (mobile phase: 30% EtOAc in pet-ether, compound **1** R_f = 0.65 and compound **2** R_f = 0.5). The reaction mixture was cooled to room temperature; the insoluble solid was dissolved in dichloromethane (200 mL) and concentrated under reduced pressure. The crude product was purified by flash column chromatography using 0–100% EtOAc in pet-ether and 0–10% MeOH in dichloromethane as eluents to afford compound **2** (10.0 g, quant. yield) as an off-white solid.

^{1}H NMR (400 MHz, DMSO-d_6): δ 12.10 (brs, 1H), 8.82 (d, J = 1.6 Hz, 1H), 8.55 (d, J = 1.6 Hz, 1H), 7.62 (t, J = 2.8 Hz, 1H), 6.63–6.62 (m, 1H), 3.89 (s, 3H) ppm; ^{13}C NMR (100 MHz, DMSO-d_6): δ 166.3, 150.2, 143.9, 129.7, 128.0, 118.9, 117.5, 101.3, 51.8 ppm; FT-IR (neat, cm^{-1}): 3130, 3008, 2854, 2567, 1836, 1708, 1608, 1581, 1438, 1325, 1284, 1172, 983, 769. HRMS (ESI+) calcd for $C_9H_9N_2O_2$ $[M + H]^+$ 177.0659, found 177.0656. HPLC: 99.81%, RT: 2.09 min; MR: 198–203 °C (Fig. S1–S6).

Methyl 3-iodo-1*H*-pyrrolo[2,3-*b*]pyridine-5-carboxylate (3). To a stirred solution of methyl 1*H*-pyrrolo[2,3-*b*]pyridine-5-carboxylate **2** (9.8 g, 55.68 mmol) in acetone (200 mL), *N*-iodosuccinimide (16.3 g, 72.38 mmol) was added portion-wise at ambient temperature. The resulting reaction mixture was stirred for 1 h, and reaction progress was monitored by TLC (mobile phase: 30% EtOAc in pet-ether; compound **2** R_f = 0.5 and compound **3** R_f = 0.55). The reaction mixture was concentrated under reduced pressure, cooled to 0 °C, and quenched with sat. $Na_2S_2O_5$ (150 mL). The precipitated solid was filtered. The solid obtained above was dried under reduced pressure to afford compound **3** (10.6 g, 63.08%) as a light brown solid.

^{1}H NMR (400 MHz, DMSO-d_6): δ 12.56 (brs, 1H), 8.82 (s, 1H), 8.18 (s, 1H), 7.89 (s, 1H), 3.91 (s, 3H) ppm; ^{13}C NMR (100 MHz, DMSO-d_6): δ 165.4, 149.5, 144.5, 132.1, 129.0, 121.0, 118.0, 55.6, 51.6 ppm; FT-IR (neat, cm^{-1}): 2841, 1847, 1708, 1604, 1575, 1431, 1321, 1174, 1001, 956, 694. HRMS (ESI+) calcd for $C_9H_8IN_2O_2$ $[M + H]^+$ 302.9625, found 302.9640. HPLC: 91.93%, RT: 3.35 min; MR: 212–217 °C (Fig. S7–S12).

Methyl 3-iodo-1-((2-(trimethylsilyl)ethoxy)methyl)-1*H*-pyrrolo[2,3-*b*]pyridine-5-carboxylate (4). To a stirred solution of methyl 3-iodo-1*H*-pyrrolo[2,3-*b*]pyridine-5-carboxylate **3** (10.1 g, 33.44 mmol) in *N*,*N*-dimethylformamide (250 mL), NaH (60% in mineral oil, 2.41 g, 60.19 mmol) was added in portions at 0 °C under an argon atmosphere. The resulting suspension was stirred for 10 min at the same temperature. To the above solution, 2-(trimethylsilyl)ethoxymethyl chloride (SEM-Cl) (7.1 mL, 1.61 g, 40.13 mmol) was added dropwise, and the reaction mixture was allowed to reach ambient temperature. The warmed solution was stirred for 2 h, and reaction progress was monitored by TLC (mobile phase: 20% EtOAc in pet-ether, compound **3** R_f = 0.25 and compound **4** R_f = 0.7) and LC-MS. The crude sample LC-MS showed consumption of compound **3** and formation of an equal amount of the desired product (**4**) and ester hydrolysis product (**5**). The reaction mixture was cooled to 0 °C, quenched with water (50 mL), and concentrated under reduced pressure to afford a crude mixture of compound **4** and compound **5** (16.8 g) as a brown gum.

LC-MS of **4** (47%) (ESI+) calcd for $C_{15}H_{22}IN_2O_3Si$ $[M + H]^+$ 433.05, found 433.09 and LC-MS of **5** (29%) (ESI+) calcd for $C_{14}H_{20}IN_2O_3Si$ $[M + H]^+$ 419.03, found 419.05 (Fig. S13).

3-Iodo-1-((2-(trimethylsilyl)ethoxy)methyl)-1*H*-pyrrolo[2,3-*b*]pyridine-5-carboxylic acid (5). To a stirred mixture of methyl 3-iodo-1-((2-(trimethylsilyl)ethoxy)methyl)-1*H*-pyrrolo[2,3-*b*]pyridine-5-carboxylate **4** and 3-iodo-1-((2-(trimethylsilyl)ethoxy)methyl)-1*H*-pyrrolo[2,3-*b*]pyridine-5-carboxylic acid **5** (16.8 g, 38.88 mmol) in a mixture of THF (170 mL), MeOH (85 mL) and water (85 mL), NaOH (9.33 g, 233.33 mmol) was added in three portions at 0 °C. The resulting reaction mixture was allowed to reach ambient temperature and then stirred for 3 h. Reaction progress was monitored by TLC (mobile phase: 70% EtOAc in pet-ether; compound **4** R_f = 0.7 and compound **5** R_f = 0.25) and LC-MS. The excess MeOH was removed under reduced pressure, and impurities were extracted with ethyl acetate (2 × 150 mL). The aqueous layer was cooled to 0 °C, acidified with saturated $KHSO_4$ solution (pH = 3–4) and extracted with ethyl acetate (2 × 100 mL). The combined organic layer was dried over anhydrous

Na_2SO_4 and concentrated under reduced pressure. The crude product was purified by GRACE flash chromatography on a 320 g silica column using 0–100% EtOAc in pet-ether and 0–10% MeOH in dichloromethane as the eluent, affording the pure form of compound **5** (9.48 g, 58.32%) as an off-white solid and the impure form of compound **5** (8.5 g, containing polar impurities) as a light brown solid.

^{1}H NMR (400 MHz, DMSO-d_6): δ 13.17 (brs, 1H), 8.85 (d, J = 2.0 Hz, 1H), 8.18 (d, J = 1.6 Hz, 1H), 8.05 (s, 1H), 5.64 (s, 2H), 3.52 (dt, J = 8.0 Hz, 3.2 Hz, 2H), 0.83 (dt, J = 8.0 Hz, 3.2 Hz, 2H), −0.11 (s, 9H) ppm; ^{13}C NMR (100 MHz, DMSO-d_6): δ 166.7, 149.1, 145.4, 135.1, 130.2, 122.0, 120.3, 72.5, 65.7, 57.1, 17.0, −1.4 ppm; FT-IR (neat, cm^{-1}): 2952, 1681, 1600, 1506, 1422, 1369, 1250, 1091, 835, 780; HRMS (ESI+) calcd for $C_{14}H_{20}IN_2O_3Si$ [M + H]$^+$ 419.0282, found 419.0280. HPLC: 88.79%, RT: 5.06 min; MR: 140–145 °C (Fig. S14–S19).

***N*-(4-(Chlorodifluoromethoxy)phenyl)-3-iodo-1-((2-(trimethylsilyl)ethoxy)methyl)-1*H*-pyrrolo[2,3-*b*]pyridine-5-carboxamide (7).** To a stirred solution of 3-iodo-1-((2-(trimethylsilyl)ethoxy)methyl)-1*H*-pyrrolo[2,3-*b*]pyridine-5-carboxylic acid **5** (8.0 g, 19.14 mmol), 4-(chlorodifluoromethoxy)aniline **6** (3.17 mL, 22.96 mmol) and Et_3N (7.99 mL, 57.42 mmol) in *N*,*N*-dimethylformamide (80 mL), HATU (8.73 g, 22.96 mmol) was added in two portions at 0 °C under an argon atmosphere. The resulting reaction mixture was allowed to reach ambient temperature and then stirred for 3 h. The reaction progress was monitored by LC-MS. The reaction mixture was cooled to 0 °C, quenched with saturated $NaHCO_3$ (200 mL), and extracted with ethyl acetate (2 × 120 mL). The combined organic layer was dried over anhydrous Na_2SO_4 and then concentrated under reduced pressure. The crude product was purified by GRACE flash chromatography using a 220 g C18 column and 0–100% acetonitrile in 0.1% formic acid in water as the eluent. The combined fractions were mixed and basified with saturated $NaHCO_3$ (pH = 8–9), and excess acetonitrile was removed under reduced pressure. The precipitated solid was extracted with ethyl acetate (2 × 100 mL). The combined organic layer was dried over anhydrous Na_2SO_4 and then concentrated under reduced pressure to afford compound **7** (9.45 g, 83.20%) as an off-white solid.

^{1}H NMR (400 MHz, DMSO-d_6): δ 10.62 (brs, 1H), 8.91 (d, J = 2.0 Hz, 1H), 8.36 (d, J = 2.0 Hz, 1H), 8.05 (s, 1H), 7.94–7.90 (m, 2H), 7.37 (d, J = 8.8 Hz, 2H), 5.66 (s, 2H), 3.53 (t, J = 8.0 Hz, 2H), 0.82 (t, J = 8.0 Hz, 2H), −0.09 (s, 9H) ppm; ^{13}C NMR (100 MHz, DMSO-d_6): δ 164.6, 148.6, 145.0, 144.3, 138.3, 135.0, 128.5, 124.9 (t, J = 285.0 Hz, CF_2Cl), 124.0, 121.8, 121.71, 1.25.0, 124.9 (t, J = 284.9 Hz, CF_2Cl), 121.8, 121.7, 72.5, 65.7, 57.0, 17.0, −1.4 ppm; ^{19}F NMR (376 MHz, DMSO-d_6) δ −24.69; FT-IR (neat, cm^{-1}): 3539, 3315, 1890, 1728, 1620, 1552, 1502, 1089, 1018, 937, 833, 777. HRMS (ESI+) calcd for $C_{21}H_{24}ClF_2IN_3O_3Si$ [M + H]$^+$ 594.0283, found 594.0256. HPLC: 94.14%, RT: 14.11 min; MR: 115–120 °C (Fig. S20–S26).

General procedure A for Suzuki coupling reaction: synthesis of 8a–p

To a 5 minute pre-stirred argon-purged solution of *N*-(4-(chlorodifluoromethoxy)phenyl)-3-iodo-1-((2-(trimethylsilyl)ethoxy)methyl)-1*H*-pyrrolo[2,3-*b*]pyridine-5-carboxamide **7** (0.3 g, 0.505 mmol), arylboronic acid/ester (1.01 mmol), and Cs_2CO_3 (492.8 mg, 1.52 mmol) in a mixture of 1,4-dioxane (8.0 mL) and water (2.5 mL), Pd(dppf)Cl_2·DCM complex (41.3 mg, 0.051 mmol) was added at ambient temperature. The resulting mixture was irradiated at 120 °C for 2 h in a microwave. The reaction progress was monitored by LC-MS. The reaction mixture was cooled to rt and the dark brown layer was separated. The collected layer was concentrated under reduced pressure to afford compounds **8a–p** (0.43 g to 0.49 g). The crude product was used directly in the next step without further purification.

***N*-(4-(Chlorodifluoromethoxy)phenyl)-3-(1-(tetrahydro-2*H*-pyran-2-yl)-1*H*-pyrazol-5-yl)-1-((2-(trimethylsilyl)ethoxy)methyl)-1*H*-pyrrolo[2,3-*b*]pyridine-5-carboxamide (8a).** This compound was prepared according to General procedure-A, using compound 7 and 1-(tetrahydro-2*H*-pyran-2-yl)-5-(4,4,5,5-tetramethyl-1,3,2-dioxaborolan-2-yl)-1*H*-pyrazole as the boronic ester, to afford compound **8a** (0.44 g, crude) as a light brown solid.

LC-MS (ESI+) calcd for $C_{29}H_{34}ClF_2N_5O_4Si$ [M + H]$^+$ 618.21, found 618.52 (Fig. S27).

***N*-(4-(Chlorodifluoromethoxy)phenyl)-3-(pyrazin-2-yl)-1-((2-(trimethylsilyl)ethoxy)-methyl)-1*H*-pyrrolo[2,3-*b*]pyridine-5-carboxamide (8b).** This compound was prepared according to General procedure-A using compound 7 and pyrazin-2-ylboronic acid as the boronic acid to afford compound **8b** (0.43 g, crude) as a light brown solid.

LC-MS (ESI+) calcd for $C_{25}H_{27}ClF_2N_5O_3Si$ [M + H]$^+$ 546.15, found 546.39 (Fig. S28).

***N*-(4-(Chlorodifluoromethoxy)phenyl)-3-(pyrimidin-5-yl)-1-((2-(trimethylsilyl)ethoxy)methyl)-1*H*-pyrrolo[2,3-*b*]pyridine-5-carboxamide (8c).** This compound was prepared according to General procedure-A using compound 7 and pyrimidin-5-ylboronic acid as the boronic acid to afford compound **8c** (0.45 g, crude) as a light brown solid.

LC-MS (ESI+) calcd for $C_{25}H_{27}ClF_2N_5O_3Si$ [M + H]$^+$ 546.15, found 546.39 (Fig. S29).

***N*-(4-(Chlorodifluoromethoxy)phenyl)-3-(6-methoxypyridin-3-yl)-1-((2-(trimethylsilyl)-ethoxy)methyl)-1*H*-pyrrolo[2,3-*b*] pyridine-5-carboxamide (8d).** This compound was prepared according to General procedure-A using compound 7 and (6-methoxypyridin-3-yl)boronic acid as the boronic acid to afford compound **8d** (0.44 g, crude) as a dark brown solid.

LC-MS (ESI+) calcd for $C_{27}H_{30}ClF_2N_4O_4Si$ [M + H]$^+$ 575.17, found 575.42 (Fig. S30).

***N*-(4-(Chlorodifluoromethoxy)phenyl)-3-(2-methoxypyridin-3-yl)-1-((2-(trimethylsilyl)-ethoxy)methyl)-1*H*-pyrrolo[2,3-*b*] pyridine-5-carboxamide (8e).** This compound was prepared according to General procedure-A using compound 7 and (2-methoxypyridin-3-yl)boronic acid as the boronic acid to afford compound **8e** (0.46 g, crude) as a dark brown solid.

LC-MS (ESI+) calcd for $C_{27}H_{30}ClF_2N_4O_4Si$ [M + H]$^+$ 575.17, found 575.42 (Fig. S31).

***N*-(4-(Chlorodifluoromethoxy)phenyl)-3-(2-methoxypyridin-4-yl)-1-((2-(trimethylsilyl) ethoxy)methyl)-1*H*-pyrrolo[2,3-*b*] pyridine-5-carboxamide (8f).** This compound was prepared

according to General procedure-A using compound 7 and (2-methoxypyridin-4-yl)boronic acid as the boronic acid to afford compound **8f** (0.47 g, crude) as a light brown solid.

LC-MS (ESI+) calcd for $C_{27}H_{30}ClF_2N_4O_4Si$ $[M + H]^+$ 575.17, found 575.46 (Fig. S32).

***N*-(4-(Chlorodifluoromethoxy)phenyl)-3-(2,6-dimethoxypyridin-4-yl)-1-((2-(trimethylsilyl)ethoxy)methyl)-1*H*-pyrrolo[2,3-*b*]pyridine-5-carboxamide (8g).** This compound was prepared according to General procedure-A using compound 7 and (2,6-dimethoxypyridin-4-yl)boronic acid as the boronic acid to afford compound **8g** (0.48 g, crude) as a dark brown solid.

LC-MS (ESI+) calcd for $C_{28}H_{32}ClF_2N_4O_5Si$ $[M + H]^+$ 605.18, found 605.45 (Fig. S33).

***N*-(4-(Chlorodifluoromethoxy)phenyl)-3-(5-methoxypyridin-3-yl)-1-((2-(trimethylsilyl)-ethoxy)methyl)-1*H*-pyrrolo[2,3-*b*]pyridine-5-carboxamide (8h).** This compound was prepared according to General procedure-A using compound 7 and (5-methoxypyridin-3-yl)boronic acid as the boronic acid to afford compound **8h** (0.47 g, crude) as a light brown solid.

LC-MS (ESI+) calcd for $C_{27}H_{30}ClF_2N_4O_4Si$ $[M + H]^+$ 575.17, found 575.46 (Fig. S34).

***N*-(4-(Chlorodifluoromethoxy)phenyl)-3-(6-ethoxypyridin-3-yl)-1-((2-(trimethylsilyl)-ethoxy)methyl)-1*H*-pyrrolo[2,3-*b*]pyridine-5-carboxamide (8j).** This compound was prepared according to General procedure-A using compound 7 and (6-ethoxypyridin-3-yl)boronic acid as the boronic acid to afford compound **8j** (0.47 g, crude) as a light brown solid.

LC-MS (ESI+) calcd for $C_{28}H_{32}ClF_2N_4O_4Si$ $[M + H]^+$ 589.18, found 589.45 (Fig. S35).

***N*-(4-(Chlorodifluoromethoxy)phenyl)-3-(pyridin-3-yl)-1-((2-(trimethylsilyl)-ethoxy)methyl)-1*H*-pyrrolo[2,3-*b*]pyridine-5-carboxamide (8k).** This compound was prepared according to General procedure-A using compound 7 and pyridin-3-ylboronic acid as the boronic acid to afford compound **8k** (0.48 g, crude) as a light brown solid.

LC-MS (ESI+) calcd for $C_{26}H_{28}ClF_2N_4O_3Si$ $[M + H]^+$ 545.16, found 545.42 (Fig. S36).

***N*-(4-(Chlorodifluoromethoxy)phenyl)-3-(pyridin-4-yl)-1-((2-(trimethylsilyl)-ethoxy)methyl)-1*H*-pyrrolo[2,3-*b*]pyridine-5-carboxamide (8l).** This compound was prepared according to General procedure-A using compound 7 and pyridin-4-ylboronic acid as the boronic acid to afford compound **8l** (0.45 g, crude) as a dark brown solid.

LC-MS (ESI+) calcd for $C_{26}H_{28}ClF_2N_4O_3Si$ $[M + H]^+$ 545.16, found 545.46 (Fig. S37).

***N*-(4-(Chlorodifluoromethoxy)phenyl)-3-(5-methylpyridin-3-yl)-1-((2-(trimethylsilyl)-ethoxy)methyl)-1*H*-pyrrolo[2,3-*b*]pyridine-5-carboxamide (8m).** This compound was prepared according to General procedure-A using compound 7 and (5-methylpyridin-3-yl)boronic acid as the boronic acid to afford compound **8m** (0.48 g, crude) as a dark brown solid.

LC-MS (ESI+) calcd for $C_{27}H_{30}ClF_2N_4O_3Si$ $[M + H]^+$ 559.17, found 559.45 (Fig. S38).

***N*-(4-(Chlorodifluoromethoxy)phenyl)-3-phenyl-1-((2-(trimethylsilyl)ethoxy)methyl)-1*H*-pyrrolo[2,3-*b*]pyridine-5-carboxamide (8n).** This compound was prepared according to General procedure-A using compound 7 and phenylboronic acid as the boronic acid to afford compound **8n** (0.44 g, crude) as a dark brown solid.

LC-MS (ESI+) calcd for $C_{27}H_{29}ClF_2N_3O_3Si$ $[M + H]^+$ 544.16, found 544.41 (Fig. S39).

***N*-(4-(Chlorodifluoromethoxy)phenyl)-3-(quinolin-3-yl)-1-((2-(trimethylsilyl)-ethoxy)methyl)-1*H*-pyrrolo[2,3-*b*]pyridine-5-carboxamide (8p).** This compound was prepared according to General procedure-A using compound 7 and quinolin-3-ylboronic acid as the boronic acid to afford compound **8p** (0.48 g, crude) as a dark brown solid.

LC-MS (ESI+) calcd for $C_{30}H_{30}ClF_2N_4O_3Si$ $[M + H]^+$ 595.17, found 595.25 (Fig. S40).

General Procedure-B for SEM group deprotection 9a–p

To a solution of compound **8a–p** (0.43 g to 0.49 g, crude) in dichloromethane (5.0 mL), TFA (5.0 mL) was added dropwise at 0 °C. The resulting solution was allowed to warm to rt and stirred for 18 h. The reaction mixture was concentrated under reduced pressure, and the crude was dissolved in MeOH (5 mL) at 0 °C. 25% NH_3 in water (5 mL) was added dropwise at 0 °C, and the mixture was stirred for 16 h at rt. The reaction progress was monitored by LC-MS. The reaction mixture was concentrated under reduced pressure to afford the crude compounds **9a–p**.

Note: the overall two-step yield is mentioned here.

***N*-(4-(Chlorodifluoromethoxy)phenyl)-3-(1*H*-pyrazol-5-yl)-1*H*-pyrrolo[2,3-*b*]pyridine-5-carboxamide (9a).** This compound was prepared according to General procedure-B, and the crude product was purified by BUCHI flash chromatography using a 40 g C18 column and 0–100% acetonitrile in 0.1 mM ammonium bicarbonate in water as an eluent to afford compound **9a** (80 mg, 39.17%) as an off-white solid.

^{1}H NMR (400 MHz, DMSO-d_6): δ 13.06 (brs, 1H), 12.11 (brs, 1H), 10.59 (s, 1H), 9.04 (brs, 1H), 8.86 (d, $J = 1.6$ Hz, 1H), 7.98–7.92 (m, 3H), 7.77 (brs, 1H), 7.37 (d, $J = 9.2$ Hz, 2H), 6.71 (s, 1H), 6.84 (s, 1H) ppm; ^{13}C NMR (100 MHz, DMSO-d_6): δ 165.5, 149.8, 144.9, 143.0, 138.6, 129.3, 125.0, 124.7, 122.9, 122.1, 121.8, 121.5, 109.9, 101.6 ppm; ^{19}F NMR (376 MHz, DMSO-d_6) δ −24.67; FT-IR (neat, cm^{-1}): 3577, 3277, 1631, 1516, 1396, 1305, 1209, 1139, 1022, 873, 825, 758, 619. HRMS (ESI+) calcd for $C_{18}H_{13}ClF_2N_5O_2$ $[M + H]^+$ 404.0720, found 404.0694. HPLC: 95.09%, RT: 8.84 min; MR: 280–285 °C (Fig. S41–S47).

***N*-(4-(Chlorodifluoromethoxy)phenyl)-3-(pyrazin-2-yl)-1*H*-pyrrolo[2,3-*b*]pyridine-5-carboxamide (9b).** This compound was prepared according to General procedure-B, and the crude product was purified by BUCHI flash chromatography using a 40 g C18 column and 0–60% acetonitrile in 0.1 mM ammonium bicarbonate in water as an eluent to afford compound **9b** (22 mg, 10.46%) as an off-white solid.

^{1}H NMR (400 MHz, DMSO-d_6): δ 12.63 (brs, 1H), 10.65 (s, 1H), 9.29 (d, $J = 1.6$ Hz, 2H), 8.93 (d, $J = 2.0$ Hz, 1H), 8.69 (s, 1H), 8.59 (s, 1H), 8.44 (d, $J = 2.4$ Hz, 1H), 7.94 (d, $J = 8.8$ Hz, 2H), 7.38 (d, $J = 8.8$ Hz, 2H) ppm; ^{13}C NMR (100 MHz, DMSO-d_6): δ 165.3, 150.4, 150.2, 143.9, 143.7, 141.7, 140.8, 139.7, 138.5, 130.0, 128.6, 123.9, 121.8, 121.6, 116.7, 112.0 ppm; ^{19}F NMR (376 MHz, DMSO-d_6) δ −24.68; FT-IR (neat, cm^{-1}): 3599, 3236, 1635, 1398, 1317, 1217, 1139, 1022, 827, 779, 717, 646. HRMS (ESI+) calcd

for $C_{19}H_{13}ClF_2N_5O_2$ $[M + H]^+$ 416.0720, found 416.0697. HPLC: 96.01%, RT: 9.38 min; MR: 115–120 °C (Fig. S48–S54).

***N*-(4-(Chlorodifluoromethoxy)phenyl)-3-(pyrimidin-5-yl)-1*H*-pyrrolo[2,3-*b*]pyridine-5-carboxamide (9c).** This compound was prepared according to General procedure-B, and the crude product was purified by BUCHI flash chromatography using a 40 g C18 column and 0–65% acetonitrile in 0.1 mM ammonium bicarbonate in water as an eluent to afford compound **9c** (60 mg, 28.53%) as a white solid.

^{1}H NMR (400 MHz, DMSO-d_6): δ 12.59 (brs, 1H), 10.54 (s, 1H), 9.32 (s, 2H), 9.13 (s, 1H), 8.96–8.92 (m, 2H), 8.31 (s, 1H), 7.92 (d, J = 8.0 Hz, 2H), 7.39 (d, J = 8.0 Hz, 2H) ppm; ^{13}C NMR (100 MHz, DMSO-d_6): δ 165.0, 155.8, 153.8, 150.2, 145.0, 144.1, 138.3, 128.7, 127.3, 127.0, 124.9 (t, J = 285.1 Hz, CF_2Cl), 123.1, 121.8, 115.7, 108.6 ppm; ^{19}F NMR (376 MHz, DMSO-d_6) δ −24.69; FT-IR (neat, cm^{-1}): 3500, 1678, 1620, 1510, 1408, 1305, 1205, 1138, 1028, 918, 875, 827, 727, 628. HRMS (ESI+) calcd for $C_{19}H_{13}ClF_2N_5O_2$ $[M + H]^+$ 416.0720, found 416.0690. HPLC: 99.75%, RT: 8.78 min; MR: 335–340 °C (Fig. S55–S61).

***N*-(4-(Chlorodifluoromethoxy)phenyl)-3-(6-methoxypyridin-3-yl)-1*H*-pyrrolo[2,3-*b*]pyridine-5-carboxamide (9d).** This compound was prepared according to General procedure-B, and the crude product was purified by BUCHI flash chromatography using a 40 g C18 column and 0–70% acetonitrile in 0.1 mM ammonium bicarbonate in water as an eluent to afford compound **9d** (160 mg, 71.10%) as an off-white solid.

^{1}H NMR (400 MHz, DMSO-d_6): δ 12.31 (brs, 1H), 10.54 (brs, 1H), 8.90–8.66 (m, 3H), 8.12–7.92 (m, 4H),7.53–7.38 (m, 2H), 6.96 (d, J = 6.0 Hz, 1H), 3.92 (s, 3H) ppm; ^{13}C NMR (100 MHz, DMSO-d_6): δ 165.2, 162.0, 150.1, 144.9, 144.1, 143.6, 138.4, 137.5, 127.1, 125.0, 124.9 (t, J = 285.1 Hz, CF_2Cl), 123.9, 122.6, 122.1, 121.7, 116.0, 112.1, 110.7, 53.1 ppm; ^{19}F NMR (376 MHz, DMSO-d_6) δ −24.69; FT-IR (neat, cm^{-1}): 3562, 3481, 3408, 3286, 2879, 1645, 1519, 1390, 1298, 1207, 1139, 1018, 883, 823, 771, 628. HRMS (ESI+) calcd for $C_{21}H_{16}ClF_2N_4O_3$ $[M + H]^+$ 445.0874, found 445.0870. HPLC: 93.67%, RT: 10.42 min; MR: 250–255 °C (Fig. S62–S68).

***N*-(4-(Chlorodifluoromethoxy)phenyl)-3-(2-methoxypyridin-3-yl)-1*H*-pyrrolo[2,3-*b*]pyridine-5-carboxamide (9e).** This compound was prepared according to General procedure-B, and the crude product was purified by BUCHI flash chromatography using a 40 g C18 column and 0–70% acetonitrile in 0.1 mM ammonium bicarbonate in water as an eluent to afford compound **9e** (130 mg, 57.77%) as an off-white solid.

^{1}H NMR (400 MHz, DMSO-d_6): δ 12.33 (brs, 1H), 10.50 (s, 1H), 8.89 (s, 1H), 8.71 (s, 1H), 8.15–8.07 (m, 2H), 7.97 (s, 1H), 7.92 (d, J = 8.4 Hz, 2H), 7.37 (d, J = 8.4 Hz, 2H), 7.14 (t, J = 8.0 Hz, 1H), 3.96 (s, 3H) ppm; ^{13}C NMR (100 MHz, DMSO-d_6): δ 165.3, 160.0, 149.8, 144.9, 144.1, 143.2, 138.5, 137.4, 128.0, 127.7, 124.9 (t, J = 285.5 Hz, CF_2Cl), 122.6, 121.8, 121.6, 117.3, 117.3, 117.0, 109.8, 53.2 ppm; ^{19}F NMR (376 MHz, DMSO-d_6) δ −24.69; FT-IR (neat, cm^{-1}): 3419, 1639, 1510, 1462, 1404, 1348, 1205, 1145, 1022, 927, 783, 719, 613. HRMS (ESI+) calcd for $C_{21}H_{16}ClF_2N_4O_3$ $[M + H]^+$ 445.0874, found 445.0864. HPLC: 97.51%, RT: 10.40 min; MR: 255–260 °C (Fig. S69–S75).

***N*-(4-(Chlorodifluoromethoxy)phenyl)-3-(2-methoxypyridin-4-yl)-1*H*-pyrrolo[2,3-*b*]pyridine-5-carboxamide (9f).** This compound was prepared according to General procedure-B, and the crude product was purified by BUCHI flash chromatography using a 40 g C18 column and 0–70% acetonitrile in 0.1 mM ammonium bicarbonate in water as an eluent to afford compound **9f** (95 mg, 42.22%) as a white solid.

^{1}H NMR (400 MHz, DMSO-d_6): δ 12.57 (brs, 1H), 10.61 (s, 1H), 8.90 (s, 2H), 8.32 (s, 1H), 8.22 (d, J = 5.6 Hz, 1H), 7.93 (d, J = 8.8 Hz, 2H), 7.47 (d, J = 5.2 Hz, 1H), 7.39 (d, J = 4.8 Hz, 2H), 7.26 (s, 1H), 3.96 (s, 3H) ppm; ^{13}C NMR (100 MHz, DMSO-d_6): δ 165.2, 164.4, 150.4, 147.2, 145.0, 144.8, 143.7, 138.4, 128.0, 127.5, 124.9 (t, J = 285.3 Hz, CF_2Cl), 123.3, 121.8, 121.7, 115.9, 114.8, 112.6, 106.3, 4.3, 53.0 ppm; ^{19}F NMR (376 MHz, DMSO-d_6) δ −24.68; FT-IR (neat, cm^{-1}): 3564, 3398, 3234, 1620, 1527, 1394, 1311, 1209, 1134, 1037, 995, 821, 615. HRMS (ESI+) calcd for $C_{21}H_{16}ClF_2N_4O_3$ $[M + H]^+$ 445.0874, found 445.0866. HPLC: 99.02%, RT: 10.21 min; MR: 270–275 °C (Fig. S76–S82).

***N*-(4-(Chlorodifluoromethoxy)phenyl)-3-(2,6-dimethoxypyridin-4-yl)-1*H*-pyrrolo[2,3-*b*]pyridine-5-carboxamide (9g).** This compound was prepared according to General procedure-B, and the crude product was purified by BUCHI flash chromatography using a 40 g C18 column and 0–90% acetonitrile in 0.1 mM ammonium bicarbonate in water as an eluent to afford compound **9g** (85 mg, 35.38%) as an off-white solid.

^{1}H NMR (400 MHz, DMSO-d_6): δ 12.19 (brs, 1H), 10.47 (s, 1H), 8.87 (d, J = 2.0 Hz, 1H), 8.63 (d, J = 2.0 Hz, 1H), 7.97 (d, J = 8.0 Hz, 1H), 7.92 (d, J = 8.8 Hz, 2H), 7.81 (s, 1H), 7.37 (d, J = 8.8 Hz, 2H), 6.53 (d, J = 8.0 Hz, 1H), 3.96 (s, 3H), 3.92 (s, 3H) ppm; ^{13}C NMR (100 MHz, DMSO-d_6): δ 165.3, 160.8, 158.7, 149.6, 144.9, 143.0, 140.9, 138.5, 127.9, 126.4, 124.9 (t, J = 285.1 Hz, CF_2Cl), 122.3, 121.8, 121.5, 117.2, 110.0, 108.6, 101.0, 53.2, 53.1 ppm; ^{19}F NMR (376 MHz, DMSO-d_6) δ −24.69; FT-IR (neat, cm^{-1}): 3244, 1654, 1604, 1504, 1456, 1319, 1211, 1022, 831. HRMS (ESI+) calcd for $C_{22}H_{18}ClF_2N_4O_4$ $[M + H]^+$ 475.0979, found 475.0982. HPLC: 99.64%, RT: 11.40 min; MR: 258–263 °C (Fig. S83–S89).

***N*-(4-(Chlorodifluoromethoxy)phenyl)-3-(5-methoxypyridin-3-yl)-1*H*-pyrrolo[2,3-*b*]pyridine-5-carboxamide (9h).** This compound was prepared according to General procedure-B, and the crude product was purified by BUCHI flash chromatography using a 40 g C18 column and 0–80% acetonitrile in 0.1 mM ammonium bicarbonate in water as an eluent to afford compound **9h** (80 mg, 35.55%) as a white solid.

^{1}H NMR (400 MHz, DMSO-d_6): δ 12.45 (brs, 1H), 10.57 (s, 1H), 8.90 (s, 2H), 8.70 (d, J = 1.6 Hz, 1H), 8.25 (d, J = 2.8 Hz, 1H), 8.19 (s, 1H), 7.95–7.90 (m, 2H), 7.74 (t, J = 2.4 Hz, 1H), 7.38 (d, J = 8.8 Hz, 2H), 3.94 (s, 3H) ppm; ^{13}C NMR (100 MHz, DMSO-d_6): δ 165.2, 155.7, 150.2, 144.9, 143.8, 139.6, 138.4, 134.9, 131.0, 127.3, 126.6, 124.9 (t, J = 284.8 Hz, CF_2Cl), 122.1, 121.7, 121.4, 117.8, 116.0, 112.0, 55.6 ppm; ^{19}F NMR (376 MHz, DMSO-d_6) δ −24.69; FT-IR (neat, cm^{-1}): 3493, 3315, 3120, 3018, 2347, 1649, 1589, 1514, 1402, 1309, 1205, 1136, 1014, 877, 709, 520. HRMS (ESI+) calcd for $C_{21}H_{16}ClF_2N_4O_3$ $[M + H]^+$ 445.0874, found 445.0857. HPLC: 99.09%, RT: 9.57 min; MR: 270–275 °C (Fig. S90–S96).

***N*-(4-(Chlorodifluoromethoxy)phenyl)-3-(6-ethoxypyridin-3-yl)-1*H*-pyrrolo[2,3-*b*]pyridine-5-carboxamide (9j).** This compound was prepared according to General procedure-B, and

the crude product was purified by BUCHI flash chromatography using a 40 g C18 column and 0–90% acetonitrile in 0.1 mM ammonium bicarbonate in water as an eluent to afford compound **9j** (70 mg, 30.16%) as an off-white solid.

^{1}H NMR (400 MHz, DMSO-d_6): δ 12.32 (s, 1H), 10.55 (s, 1H), 8.87 (d, J = 18.8 Hz, 2H), 8.64 (s, 1H), 8.11 (d, J = 7.2 Hz, 1H), 8.00–7.91 (m, 3H), 7.38 (d, J = 8.4 Hz, 2H), 6.92 (d, J = 8.4 Hz, 1H), 4.37 (q, J = 6.8 Hz, 2H), 1.36 (t, J = 6.8 Hz, 3H) ppm; ^{13}C NMR (100 MHz, DMSO-d_6): δ 165.2, 161.7, 150.1, 144.9, 144.1, 143.6, 138.4, 137.5, 127.8, 127.1, 125.0, 123.7, 122.6, 122.1, 121.8, 121.7, 116.0, 112.1, 110.8, 61.1, 14.5 ppm; ^{19}F NMR (376 MHz, DMSO-d_6) δ −24.63; FT-IR (neat, cm^{-1}): 3481, 1631, 1529, 1390, 1300, 1203, 1136, 1026, 921, 825, 777, 621. HRMS (ESI+) calcd for $C_{22}H_{18}ClF_2N_4O_3$ [M + H]$^+$ 459.1030, found 459.1029. HPLC: 98.92%, RT: 11.02 min; MR: 243–248 °C (Fig. S97–S103).

***N*-(4-(Chlorodifluoromethoxy)phenyl)-3-(pyridin-3-yl)-1*H*-pyrrolo[2,3-*b*]pyridine-5-carboxamide (9k).** This compound was prepared according to General procedure-B, and the crude product was purified by BUCHI flash chromatography using a 40 g C18 column and 0–75% acetonitrile in 0.1 mM ammonium bicarbonate in water as an eluent to afford compound **9k** (83 mg, 39.55%) as an off-white solid.

^{1}H NMR (400 MHz, DMSO-d_6): δ 12.45 (brs, 1H), 10.57 (brs, 1H), 9.08 (s, 1H), 8.90 (s, 2H), 8.52 (s, 1H), 8.36–8.16 (m, 2H), 7.93 (d, J = 7.6 Hz, 2H), 7.51 (s, 1H), 7.38 (d, J = 7.6 Hz, 1H) ppm; ^{13}C NMR (100 MHz, DMSO-d_6): δ 165.2, 150.2, 147.3, 147.0, 145.0, 143.7, 138.4, 133.5, 130.3, 127.8, 126.2, 124.9 (t, J = 284.1 Hz, CF_2Cl), 123.9, 122.1, 121.8, 121.7, 116.0, 112.1 ppm; ^{19}F NMR (376 MHz, DMSO-d_6) δ −24.69; FT-IR (neat, cm^{-1}): 3475, 3244, 2856, 1639, 1554, 1494, 1409, 1340, 1211, 1136, 1016, 790, 713, 626. HRMS (ESI+) calcd for $C_{20}H_{14}ClF_2N_4O_2$ [M + H]$^+$ 415.0768, found 415.0765. HPLC: 99.14%, RT: 9.27 min; MR: 260–265 °C (Fig. S104–S110).

***N*-(4-(Chlorodifluoromethoxy)phenyl)-3-(pyridin-4-yl)-1*H*-pyrrolo[2,3-*b*]pyridine-5-carboxamide (9l).** This compound was prepared according to General procedure-B, and the crude product was purified by BUCHI flash chromatography using a 40 g C18 column and 0–75% acetonitrile in 0.1 mM ammonium bicarbonate in water as an eluent to afford compound **9l** (77 mg, 36.69%) as a light brown solid.

^{1}H NMR (400 MHz, DMSO-d_6): δ 12.58 (brs, 1H), 10.58 (s, 1H), 8.95 (s, 1H), 8.91 (s, 1H), 8.62 (d, J = 4.8 Hz, 2H), 8.35 (s, 1H), 7.94 (d, J = 9.2 Hz, 2H), 7.86 (d, J = 5.6 Hz, 2H), 7.39 (d, J = 8.4 Hz, 2H) ppm; ^{13}C NMR (100 MHz, DMSO-d_6): δ 165.2, 150.4, 150.0, 145.0, 143.7, 141.8, 138.4, 127.9, 127.6, 124.9 (t, J = 285.1 Hz, CF_2Cl), 123.4, 121.8, 121.6, 120.5, 115.9, 112.6 ppm; ^{19}F NMR (376 MHz, DMSO-d_6) δ −24.69; FT-IR (neat, cm^{-1}): 3603, 3234, 1645, 1546, 1498, 1402, 1315, 1203, 1130, 1022, 879, 827, 775, 617. HRMS (ESI+) calcd for $C_{20}H_{14}ClF_2N_4O_2$ [M + H]$^+$ 415.0768, found 415.0758. HPLC: 98.63%, RT: 9.04 min; MR: 283–288 °C (Fig. S111–S117).

***N*-(4-(Chlorodifluoromethoxy)phenyl)-3-(5-methylpyridin-3-yl)-1*H*-pyrrolo[2,3-*b*]pyridine-5-carboxamide (9m).** This compound was prepared according to General procedure-B, and the crude product was purified by BUCHI flash chromatography using a 40 g C18 column and 0–85% acetonitrile in 0.1 mM ammonium bicarbonate in water as an eluent to afford compound **9m** (140 mg, 64.54%) as an off-white solid.

^{1}H NMR (400 MHz, DMSO-d_6): δ 12.42 (brs, 1H), 10.57 (s, 1H), 8.90–8.88 (m, 3H), 8.36 (s, 1H), 8.13 (s, 1H), 8.02 (s, 1H), 7.93 (d, J = 8.8 Hz, 2H), 7.38 (d, J = 8.8 Hz, 2H), 2.40 (s, 3H) ppm; ^{13}C NMR (100 MHz, DMSO-d_6): δ 165.2, 150.2, 147.5, 145.0, 144.6, 143.7, 138.5, 133.9, 133.1, 129.8, 127.3, 126.1, 125.0 (t, J = 285.2 Hz, CF_2Cl), 122.9, 121.8, 121.7, 116.1, 112.2, 17.9 ppm; ^{19}F NMR (376 MHz, DMSO-d_6) δ −24.69; FT-IR (neat, cm^{-1}): 3483, 3404, 3097, 2357, 1616, 1508, 1409, 1323, 1213, 1139, 1020, 867, 711. HRMS (ESI+) calcd for $C_{21}H_{16}ClF_2N_4O_2$ [M + H]$^+$ 429.0924, found 429.0924. HPLC: 93.18%, RT: 9.67 min; MR: 272–277 °C (Fig. S118–S124).

***N*-(4-(Chlorodifluoromethoxy)phenyl)-3-phenyl-1*H*-pyrrolo[2,3-*b*]pyridine-5-carboxamide (9n).** This compound was prepared according to General procedure-B, and the crude product was purified by BUCHI flash chromatography using a 40 g C18 column and 0–95% acetonitrile in 0.1 mM ammonium bicarbonate in water as an eluent to afford compound **9n** (74 mg, 35.35%) as a white solid.

^{1}H NMR (400 MHz, DMSO-d_6): δ 12.29 (brs, 1H), 10.55 (s, 1H), 8.89 (d, J = 2.0 Hz, 1H), 8.85 (d, J = 2.0 Hz, 1H), 8.00 (s, 1H), 7.95–7.91 (m, 2H), 7.81–7.79 (m, 2H), 7.49 (t, J = 7.6 Hz, 2H), 7.38 (d, J = 8.8 Hz, 2H), 7.31 (t, J = 7.6 Hz, 1H) ppm; ^{13}C NMR (100 MHz, DMSO-d_6): δ 165.3, 150.2, 144.9, 143.3, 138.5, 134.4, 128.9, 127.3, 126.6, 126.1, 125.3, 124.9 (t, J = 285.3 Hz, CF_2Cl), 122.8, 121.8, 121.6, 116.2, 115.5 ppm; ^{19}F NMR (376 MHz, DMSO-d_6) δ −24.68; FT-IR (neat, cm^{-1}): 3489, 2349, 1645, 1514, 1406, 1305, 1213, 1138, 1020, 821, 669. HRMS (ESI+) calcd for $C_{21}H_{15}ClF_2N_3O_2$ [M + H]$^+$ 414.0815, found 414.0818. HPLC: 99.57%, RT: 11.17 min; MR: 290–300 °C (Fig. S125–S131).

***N*-(4-(Chlorodifluoromethoxy)phenyl)-3-(quinolin-3-yl)-1*H*-pyrrolo[2,3-*b*]pyridine-5-carboxamide (9p).** This compound was prepared according to General procedure-B, and the crude product was purified by BUCHI flash chromatography using a 40 g C18 column and 0–90% acetonitrile in 0.1 mM ammonium bicarbonate in water as an eluent to afford compound **9p** (40 mg, 17.01%) as a yellow solid.

^{1}H NMR (400 MHz, DMSO-d_6): δ 12.52 (brs, 1H), 10.59 (brs, 1H), 9.41 (s, 1H), 9.04 (s, 1H), 8.92 (s, 1H), 8.76 (s, 1H), 8.34 (s, 1H), 8.10 (d, J = 8.0 Hz, 1H), 8.05 (d, J = 8.0 Hz, 1H), 7.95 (d, J = 8.8 Hz, 2H), 7.74 (t, J = 7.2 Hz, 1H), 7.64 (t, J = 7.6 Hz, 1H), 7.39 (d, J = 8.4 Hz, 2H) ppm; ^{13}C NMR (100 MHz, DMSO-d_6): δ 165.3, 150.3, 149.8, 146.0, 144.9, 143.8, 138.5, 130.9, 128.7, 128.0, 127.7, 127.5, 126.9, 126.6, 124.9 (t, J = 285.3 Hz, CF_2Cl), 123.1, 121.8, 121.6, 116.2, 112.2 ppm; ^{19}F NMR (376 MHz, DMSO-d_6) δ −24.68; FT-IR (neat, cm^{-1}): 3383, 2376, 2083, 1631, 1521, 1467, 1402, 1311, 1224, 1139, 1024, 889, 825, 779, 617. HRMS (ESI+) calcd for $C_{24}H_{16}ClF_2N_4O_2$ [M + H]$^+$ 465.0924, found 465.0904. HPLC: 98.77%, RT: 10.45 min; MR: 314–317 °C (Fig. S136–S138).

Biology

Cell lines were obtained from ATCC (Middlesex, UK) and DSMZ (Braunschweig, Germany). The cells were incubated at 37 °C in a humidified incubator (5% CO_2 in atmospheric air) in the recommended growth media, supplemented with 2.0 mM

glutamine (Gibco), 1.0 mM sodium pyruvate (Gibco), 1× penicillin–streptomycin solution (Diagnovum), 10% fetal calf serum (Gibco), 20.0 mM HEPES (Gibco), and 1.0 mM sodium bicarbonate (Gibco). We routinely authenticated all cell lines and tested for mycoplasma contamination every two weeks, following our laboratory's standard protocols.[19,20]

Cytotoxicity assay

The cytotoxic activity of all compounds was evaluated for anticancer activity using a 3-(4,5-dimethylthiazol-2-yl)-2,5-diphenyltetrazolium bromide (MTST) reduction assay after 72 h of treatment on a robotic high-throughput screening (HTS) platform (HighResBio, Boston, MA, USA), using a standard protocol established in our laboratory for cell lines (K562, A549, CCRF-CEM, HCT116, HCT116 $p53^{-/-}$, U2OS, BJ and MRC-5).

Statistical analysis. All biological screening experiments were performed with a minimum of six independent biological replicates ($n \geq 6$). Each biological experiment was an independent biological replicate, not a technical replicate. Values are reported as mean ± SD. No hypothesis testing procedures or inferential statistical comparisons were used in this study. IC_{50} values were obtained by fitting concentration–response curves using Dotmatics (San Diego, CA, USA) and are expressed as mean ± SD. They were calculated from at least six independent biological experiments ($n \geq 6$). The biological screening data have been stored in the IMTM Dotmatics database and the MedChemBio Portal.[21]

Molecular docking studies

To elucidate the structural determinants governing ligand recognition and to support the design of next-generation BCR-ABL1 inhibitors, we performed systematic molecular docking studies using the ICM-Pro 3.9-5a program (Molsoft).[22]

Preparation of BCR-ABL1 protein structures

We began by retrieving the high-resolution crystal structure of the BCR-ABL1 kinase domain (PDB ID: 5MO4, 2.17 Å) from the RCSB Protein Data Bank.[23] This structure contains both Asciminib and Nilotinib, co-crystallized in the myristoyl allosteric pocket and the ATP-binding site, respectively. Because the aim of our study was to identify compounds with improved allosteric-site binding relative to Asciminib, Nilotinib was removed from the ATP-binding pocket, and only the allosteric module was retained for subsequent modelling. A conserved structural water molecule, known to stabilise Asciminib binding by forming three hydrogen bonds with the ligand and residues Ala452 and Glu481, was retained in the model (Fig. 2).

Hydrogen atoms and missing heavy atoms were added to the receptor, and appropriate atom types and partial charges were assigned. The resulting structure was subjected to local energy minimisation using the conjugate-gradient algorithm with analytical derivatives in internal coordinates to optimise the receptor geometry prior to docking.

Ligand preparation

Ligands were prepared in MolSoft ICM by importing their chemical structures in SDF format. The structures were first standardised using the Clean 3D module, which corrected valence states, added hydrogen atoms, and generated initial three-dimensional geometries. We assigned protonation states at physiological pH using the Protonate tool. Each ligand was subsequently energy-minimised using the ICM force field to obtain a low-energy starting conformation. Torsional flexibility parameters and atom types were automatically assigned during the ligand-preparation workflow. The final energy-optimised ligands were then saved as ICM ligand objects for use in subsequent docking simulations.

Ligand docking

Molecular docking was performed after identifying the ligand-binding site on the target protein. The binding pocket was predicted using the ICM Pocket Finder module (Molsoft LLC),[24] which detects potential cavities by evaluating a grid-based potential map that reflects van der Waals interaction energies between the receptor surface and probe atoms. This method prioritises physicochemical interaction potentials rather than relying solely on geometric cavity definitions. Default "Pocket Finder" parameters were used for pocket identification.

After defining the binding site, molecular docking of the known inhibitor (Asciminib) was performed using the MolSoft-ICM docking engine. A grid potential map was generated and centred over the top-ranked binding pocket to guide ligand placement. During docking, the protein structure was kept rigid, whereas ligands were treated as fully flexible, allowing conformational exploration around all rotatable bonds.

The ICM docking protocol uses a biased Monte Carlo global optimisation algorithm to thoroughly sample the ligand conformational space and evaluate potential ligand-induced adjustments within the binding region. For each ligand, the lowest-energy (best-scoring) conformer was selected using the ICM docking score. The resulting protein–ligand complexes were analysed to characterise key intermolecular interactions and define the dominant binding modes within the predicted pocket.

Molecular dynamics (MD)

Molecular dynamics (MD) simulations provide important insights into the stability and reliability of predicted docking poses and enable detailed analysis of protein-ligand interaction patterns throughout the simulation. MD was performed using the OpenMM8 package with CUDA acceleration.[25] The protein-ligand complexes of the active compound **9c** and the inactive compound **9p** were prepared using CHARMM-GUI and parameterised with the CHARMM36 force field. The systems were solvated in a TIP3P water box with a 10 Å padding and neutralised with counterions to a salt concentration of 0.15 M KCl. After 1000 steps of energy minimisation, the systems were equilibrated at 300 K under NVT conditions using a Langevin integrator. Production simulations were subsequently carried out for 100 ns in the NPT ensemble at 300 K and 1 atm, using a 4 fs timestep with hydrogen mass

repartitioning, hydrogen-bond constraints, particle-mesh Ewald (PME) electrostatics, and periodic boundary conditions. Trajectory analyses, including protein and ligand RMSD and protein-ligand contact calculations, were conducted to assess the dynamic stability and binding characteristics of the complexes.

Author contributions

Pradeep B. Bhise: writing – original draft, methodology, investigation. Sandeep B. Bhise: writing – review & editing, Somnath Dasgupta, Rambabu Gundla, Shankar R. Thopate and Pravin V. Badadhe: supervision, project administration, conceptualization, investigation, data curation. Ashis Nandy: conceptualization, visualization, investigation. Sona Gurska, Petr Dzubak, Marian Hajdúch and Viswanath Das: review, resources, funding acquisition, conceptualization.

Conflicts of interest

The authors declare that they have no known competing financial interests or personal relationships that could have appeared to influence the work reported in this paper.

Abbreviations

BCR-ABL1	Breakpoint Cluster Region (BCR)-Abelson murine leukemia viral oncogene homolog 1 (ABL1)
ATP	Adenosine triphosphate
CML	Chronic myeloid leukemia
ALL	Acute lymphoblastic leukemia
TMS	Tetramethylsilane
DMF	*N*,*N*-Dimethylformamide
HRMS	High-resolution mass spectrometry
HPLC	High performance liquid chromatography
LC-MS	Liquid chromatography-mass spectroscopy
GS	Glide-scores
Sa	Surface area
MD	Molecular dynamics

Data availability

Cytotoxicity data are stored in the IMTM Dotmatics database and MedChemBio Portal (http://www.medchembio.imtm.cz) and are available from the Palacký University Olomouc authors upon reasonable request.

Supplementary information (SI): characterisation of all compounds (^{1}H NMR, ^{13}C NMR, HRMS, HPLC, FT-IR spectra, and LC-MS) and molecular docking figures. See DOI: https://doi.org/10.1039/d6ra07332h.

Acknowledgements

All biological study was supported in part by the infrastructural projects. All biological parts of the study were supported in part by the infrastructural projects (CZ-OPENSCREEN – LM2023052; EATRIS-CZ – LM2023053), the Czech biobank network (BBMRI - LM2023033), the projects National Institute for Cancer Research (Program EXCELES, ID Project No. LX22NPO5102) and National Institute for Neurological Research (Program EXCELES, ID Project No. LX22NPO5107) – Funded by the European Union – Next Generation EU from the Ministry of Education, Youth and Sports of the Czech Republic (MEYS), project Personalized Medicine: From Translational Research into Biomedical Applications (TN02000109) co-financed with the state support of the Technology Agency of the Czech Republic as part of the National Centers of Competence Program, and project SALVAGE (CZ.02.01.01/00/22_008/0004644) supported by OP JAK, with co-financing from the EU and the State Budget. Pradeep B. Bhise, Shankar R. Thopate and Pravin B. Badadhe acknowledge the Department of Chemistry, R. B. Narayanrao Borawake College, Shrirampur, Ahilyanagar, Maharashtra, India and Aragen Life Sciences Ltd, Hyderabad, India, for providing computational resources for synthesizing and characterization of all the compounds by NMR, LC-MS, HPLC, MR and FT-IR.

References

1 J. D. Rowley, *Nature*, 1973, **243**, 290–293.
2 D. Cilloni and G. Saglio, *Clin. Cancer Res.*, 2012, **18**, 930–937.
3 B. J. Druker, M. Talpaz, D. J. Resta, B. Peng, E. Buchdunger, J. M. Ford and C. L. Sawyers, *N. Engl. J. Med.*, 2001, **344**, 1031–1037.
4 N. P. Shah, J. M. Nicoll, B. Nagar, M. E. Gorre, R. L. Paquette, J. Kuriyan and C. L. Sawyers, *Cancer Cell*, 2002, **2**, 117–125.
5 H. Kantarjian, N. P. Shah, A. Hochhaus, J. Cortes, S. Shah, M. Ayala and F. Guilhot, *N. Engl. J. Med.*, 2010, **362**, 2260–2270.
6 G. Saglio, D. W. Kim, S. Issaragrisil, P. Le Coutre, G. Etienne, C. Lobo and A. Hochhaus, *N. Engl. J. Med.*, 2010, **362**, 2251–2259.
7 J. E. Cortes, D. W. Kim, J. Pinilla-Ibarz, P. Le Coutre, R. Paquette, C. Chuah and H. M. Kantarjian, *N. Engl. J. Med.*, 2013, **367**, 2075–2088.
8 F. Musumeci, M. Sanna, G. Grossi, C. Brullo, A. L. Fallacara and S. Schenone, *Curr. Med. Chem.*, 2017, **24**, 2059–2085.
9 M. S. Madhurya, V. Thakur, S. Dastari and N. Shankaraiah, *Bioorg. Chem.*, 2024, **153**, 107867.
10 E. B. Elkaeed, M. A. Abo-Ashour, A. E. El-Telbany, *et al.*, *Molecules*, 2022, **27**, 6203.
11 J. Schoepfer, W. Jahnke, G. Berellini, S. Buonamici, S. Cotesta, S. W. Cowan-Jacob, S. Dodd, P. Drueckes, D. Fabbro, T. Gabriel, J. M. Groell, R. M. Grotzfeld, A. Q. Hassan, C. Henry, V. Iyer, D. Jones, F. Lombardo, A. Loo, P. W. Manley, X. Pellé, G. Rummel, B. Salem, M. Warmuth, A. A. Wylie, T. Zoller, A. L. Marzinzik and P. Furet, *J. Med. Chem.*, 2018, **61**, 8120–8135.
12 M. Shoukier, M. Kubiak and J. Cortés, *Curr. Oncol. Rep.*, 2021, **23**(8), 91.
13 B. Leske and O. Hantschel, *Leukemia*, 2024, **38**, 2041–2045.
14 C. M. S. Tesileanu, S. Michaleas, R. Gonzalo Ruiz, S. Mariz, B. O. Fabriek, P. B. van Hennik, J. Dedorath, B. Dekic,

C. Unkrig, A. Brandt, J. Koenig, H. Enzmann, J. Delgado and F. Pignatti, *Oncologist*, 2023, **28**, 628–632.

15 (*a*) B. M. Mulik, N. Srivastava and D. Pendharkar, *ChemistrySelect*, 2024, **9**, e202304498; (*b*) P. Bhise, S. Bhise, S. Badadhe, *et al.*, *SSRN Electron. J.*, 2026, DOI: 10.2139/ssrn.6957322.

16 S. Narva, S. Chitti, B. R. Bala, M. Alvala, N. Jain and V. G. Kondapalli, Synthesis and biological evaluation of pyrrolo[2,3-b]pyridine analogues as antiproliferative agents and their interaction with calf thymus DNA, *Eur. J. Med. Chem.*, 2016, **114**, 220–231, DOI: 10.1016/j.ejmech.2016.02.059.

17 Y.-H. Liu, M. Zhu, P.-P. Lei, X.-Y. Pan and W.-N. Ma, *Oncol. Rep.*, 2021, **46**, 136.

18 P. Wu, T. E. Nielsen and M. H. Clausen, *Trends Pharmacol. Sci.*, 2015, **36**, 422–439.

19 R. Buriánová and J. Kotulová, in *Laboratory Techniques in Cellular and Molecular Medicine*, ed. J. Drábek, *et al.*, Palacký University Olomouc, Olomouc, Czech Republic, 2022, pp. 37–42.

20 J. Stránská, in *Laboratory Techniques in Cellular and Molecular Medicine*, ed. J. Drábek, *et al.*, Palacký University Olomouc, Olomouc, Czech Republic, 2022, pp. 29–36.

21 S. Gurská, in *Laboratory Techniques in Cellular and Molecular Medicine*, ed. J. Drábek, *et al.*, Palacký University Olomouc, Olomouc, Czech Republic, 2022, pp. 67–72.

22 M. Totrov and R. Abagyan, *Proteins*, 1997, (Suppl. 1), 215–220.

23 J. Schoepfer, W. Jahnke, G. Berellini, S. Buonamici, S. Cotesta, S. W. Cowan-Jacob, S. Dodd, P. Drueckes, D. Fabbro, T. Gabriel, J. M. Groell, R. M. Grotzfeld, A. Q. Hassan, C. Henry, V. Iyer, D. Jones, F. Lombardo, A. Loo, P. W. Manley, X. Pellé, G. Rummel, B. Salem, M. Warmuth, A. A. Wylie, T. Zoller, A. L. Marzinzik and P. Furet, *J. Med. Chem.*, 2018, **61**, 8120–8135.

24 J. R. Lane, P. Chubukov, W. Liu, M. Canals, V. Cherezov, R. Abagyan, R. C. Stevens and V. Katritch, *Mol. Pharmacol.*, 2013, **84**, 794–807.

25 P. Eastman, R. Galvelis, R. P. Peláez, C. R. A. Abreu, S. E. Farr, E. Gallicchio, A. Gorenko, M. M. Henry, F. Hu, J. Huang, A. Krämer, J. Michel, J. A. Mitchell, V. S. Pande, J. PGLM Rodrigues, J. Rodriguez-Guerra, A. C. Simmonett, S. Singh, J. Swails, P. Turner, Y. Wang, I. Zhang, J. D. Chodera, G. De Fabritiis and T. E. Markland, OpenMM 8: Molecular Dynamics Simulation with Machine Learning Potentials, *J. Phys. Chem. B*, 2023, **128**(1), 109–116.